5101-233
Flat-Plate
Solar Array Project

DOE/JPL-1012-90
Distribution Category UC-63b

Characterization of Grain Boundaries in Silicon

L.J. Cheng
C.M. Shyu
K.M. Stika
T. Daud
G.T. Crotty

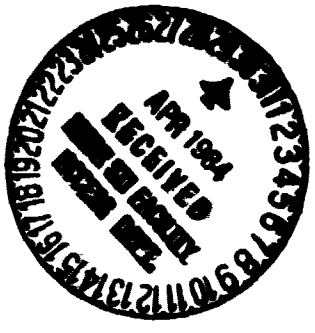

November 15, 1983

Prepared for
U.S. Department of Energy
Through an Agreement with
National Aeronautics and Space Administration
by
Jet Propulsion Laboratory
California Institute of Technology
Pasadena, California

JPL Publication 83-87

5101-233
Flat-Plate
Solar Array Project

DOE/JPL-1012-90
Distribution Category UC-63b

Characterization of Grain Boundaries in Silicon

L.J. Cheng
C.M. Shyu
K.M. Stika
T. Daud
G.T. Crotty

November 15, 1983

Prepared for
U.S. Department of Energy
Through an Agreement with
National Aeronautics and Space Administration
by

Jet Propulsion Laboratory
California Institute of Technology
Pasadena, California

JPL Publication 83-87

Prepared by the Jet Propulsion Laboratory, California Institute of Technology, for the U.S. Department of Energy through an agreement with the National Aeronautics and Space Administration.

The JPL Flat-Plate Solar Array Project is sponsored by the U.S. Department of Energy and is part of the Photovoltaic Energy Systems Program to initiate a major effort toward the development of cost-competitive solar arrays.

This publication reports on work done under NASA Task RE-152, Amendment 66, DOE / NASA IAA No. DE-AI01-76ET20356.

ABSTRACT

Results from several research activities on properties of grain boundaries in silicon materials are reported.

Zero-bias conductance and capacitance measurements at various temperatures were used to study trapped charges and potential barrier height at the boundaries. Deep-level transient spectroscopy (DLTS) was applied to measure the density of states at the boundary. The result is consistent with the model in which the density of states increases as the states become deeper. Anomalous phenomena have been observed by DLTS and other methods, which can be only explained by a new model in which the spatial distribution of the localized states is not uniform along the boundary in the microscopic scale.

A study of photoconductivity of grain boundaries in p-type silicon demonstrated the applicability of the technique in the measurement of minority carrier recombination velocity at the grain boundary. The data are consistent with the concept of recombination velocity increasing with boundary-state density and light intensity.

Enhanced diffusion of phosphorus at grain boundaries in three cast polycrystalline photovoltaic materials was studied. Enhancements for the three were the same, indicating that the properties of boundaries are similar, although grown by different techniques. Grain boundaries capable of enhancing the diffusion were found always to have strong recombination activities; The phenomena could be related to dangling bonds at the boundaries. The present study gives the first evidence that incoherent second-order twins of $\{111\}/\{115\}$ type are diffusion-active.

ACKNOWLEDGMENT

The authors thank Katherine A. Dumas, Krishna M. Koliwad and K. L. Wang for valuable technical discussions, Rindge Shima for the supply of bicrystals, and Dieter Ast for his valuable assistance in the analysis of incoherent {111}//{115} second-order twins.

CONTENTS

Figures

Tables

SECTION I

POLYCRYSTALLINE SILICON GRAIN BOUNDARIES

The grain boundary is an intrinsic part of any polycrystalline material; it plays an important role in the determination of the material's properties. Recently the increasing use of polycrystalline silicon for solar cells and other electronic devices has stimulated many investigations into the behavior of grain boundaries, which can have critical effects on device performance. To use polycrystalline silicon effectively in solar cell applications, it is necessary to improve the understanding of the grain boundary in silicon, to create innovative ideas for eliminating its degradation effects as much as possible, and to exploit it for any possible benefits.

Grain boundaries in silicon can act as majority carrier traps and minority carrier recombination centers. They can also act as gettering centers and diffusion channels for impurities. Structurally, a grain boundary is an interface between two adjoining crystals of a material with the same crystalline structure but with different lattice orientations. The lattice mismatch engenders various grain-boundary properties. There is a virtually infinite number of possible lattice mismatches between two crystals, depending not only on the difference in lattice orientation of two grains but also on the boundary direction with respect to the lattice orientation. As a result, the structure of the grain boundary is inherently complex. Any existing material can have some impurities and the grain boundary can react with impurities, making the properties of grain boundaries even more complex. This complex nature has long been recognized, and significant progress has been made in enhancing understanding of the grain boundary in silicon, not only to satisfy scientific curiosity but also to make technological advances. However, there still is a need to improve understanding in this important area; in photovoltaic (PV) applications it is necessary to improve our understanding of the effects of grain boundaries on polycrystalline silicon solar cell performance, the relationship of that performance to the structural, chemical and electrical properties of grain boundaries, and the effects of grain boundaries on cell-fabrication processes.

The Jet Propulsion Laboratory (JPL) has done a wide range of studies related to polycrystalline silicon materials and solar cells for the Flat-Plate Solar Array Project (FSA). In this report, the progress of one of the in-house research programs, which concerns silicon grain boundary characterization, is described. The electrical properties of silicon grain boundaries using zero-bias conductance and capacitance measurements were studied; these measurements provide information on majority charge density trapped at the boundaries and the potential barrier caused by the trapping. Deep-level transient spectroscopy (DLTS) has been useful in the study of localized states at the boundaries. Results show that DLTS can give vital information about the density of states of the boundary in the energy gap. Because of the existence of the localized states, the grain boundaries can trap majority carriers and act as minority carrier recombination centers. The localized states are important, because they are created by the lattice mismatch and dictate the electrical properties of boundaries. The photoconductivity of the grain boundaries has also been studied with the

objective of improving understanding of light effects on the boundary and of the boundary's influence on solar-cell performance. From the study, we have developed a new photoconductivity decay method to measure the minority carrier recombination velocity at the grain boundary. Experimental results indicate that the recombination velocity increases with the density of localized states at the boundary and with light intensity. Enhanced diffusion at boundaries in cast polycrystalline photovoltaic materials also was studied, using secondary ion mass spectroscopy, groove-and-stain technique, chemical etching, and the electron-beam induced-current (EBIC) method with the scanning electron microscope. It was found that the enhancements for several cast materials are the same, indicating that the general properties of boundaries are similar, even when grown by different techniques. It has been observed that grain boundaries capable of enhancing the diffusion always have strong recombination activity. Both phenomena may be related to lattice mismatch at the boundaries.

This report has five sections. In Section II, studies of electrical properties of grain boundaries are described. Section III describes investigations of localized states at the boundary; an account of work on the photoconductivity of grain boundaries is offered in Section IV, and in Section V, results from studies of enhanced diffusion of phosphorus at boundaries are presented.

SECTION II

ELECTRICAL PROPERTIES OF GRAIN BOUNDARIES IN SILICON BICRYSTALS

A. INTRODUCTION

The existence of intrinsic and extrinsic disorders at the grain boundary in silicon due to lattice mismatch can give rise to localized states in the band gap. Because of these localized states, the boundary can trap majority carriers. Consequently, the excess charge creates a potential barrier at the boundary for majority carriers, and depletion regions at both sides of the boundary. The resistance of the boundary is usually an exponential function of the reciprocal of temperature. A grain boundary can also be considered as two Schottky diodes in series but opposite to each other. The grain boundary thus has its own unique electrical properties.

Researchers at Sandia National Laboratories recently reported on their study of the electrical properties of grain boundaries in neutron-transmutation-doped silicon bicrystals using conductance and capacitance techniques (References 1 through 4). The neutron transmutation process gives silicon crystals a uniform distribution of phosphorus atoms and the donor concentration can be estimated accurately using reaction cross-section data. However, neutron irradiation does substantial lattice damage, and removal of the damage requires high-temperature annealing. The properties of the grain boundary usually depend on the method of material preparation and its history of heat treatments; thus it is clear that the properties of grain boundaries in neutron transmutation-doped silicon cannot be representative of grain boundaries in polycrystalline material grown and doped from the melt. In addition, the commonly used silicon solar cell material is boron-doped, not phosphorus-doped, p-type silicon.

In this section the results of a study of grain boundaries in Cz-grown bicrystals using temperature dependence measurements of zero-bias conductance and DLTS are reported. The temperature dependence provides information concerning the carrier transport process across the boundary. By measuring samples cut sequentially along a grain boundary, variations in carrier transport along the boundary were studied.

B. EXPERIMENTAL PROCEDURES

Samples were cut from a Cz-grown boron-doped silicon ingot of 30 ohm-cm resistivity, consisting largely of bicrystalline Si. The growth directions of the two crystals in the bicrystal were [221], but rotated about 160 deg with respect to each other. The ingot was first sliced into wafers along the direction perpendicular to the growth direction. The bicrystalline parts of two wafers were cut into bar-shaped samples with the grain boundary across the middle of each. Two ohmic contacts were then made on each side of the boundary by aluminum evaporation followed by sintering at 550°K. in a hydrogen atmosphere for 6 min. After the contacts were made, the middle portion of the sample including the boundary was etched again to eliminate any undesired surface effects. During the measurements, the sample was mounted in

a variable-temperature cryostat with provision for adjusting the sample temperature to any value, within 0.1 deg, in the range from 90°K to 300°K.

The system used to measure zero-bias conductance consisted of a Keithley 225 current source and a Keithley 600B electrometer. During the measurements, the sample was in darkness and the voltage across the boundary was maintained at a value of 5 mV or lower to ensure that the measured value would represent the true value of zero-bias boundary conductance.

C. RESULTS AND DISCUSSION

Figure 1 displays Arrhenius plots of zero-bias conductance data measured on three bicrystal samples. The data on sample No. 52 reveal that the temperature dependence of the sample's zero-bias conductance has one thermal activation energy of 0.55 eV. But the data for samples No. 53 and

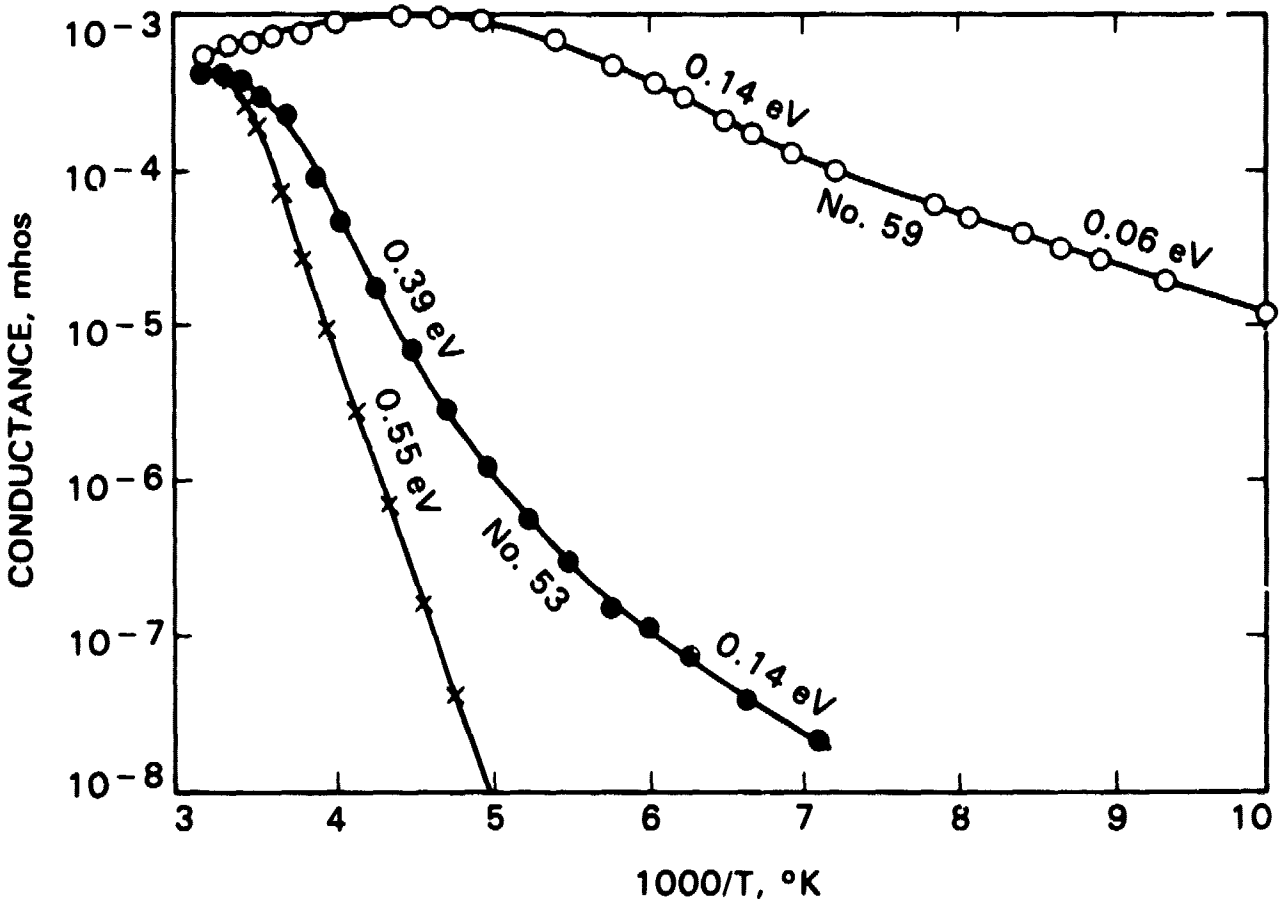

Figure 1. Zero-Bias Conductance of Three Bicrystal Samples as Functions of Reciprocal of Temperature

No. 59 show that each sample has two thermal activation energies for carrier transport over its grain boundary: 0.39 eV and 0.14 eV for sample No. 53, and 0.14 and 0.06 eV for sample No. 59.

According to the double-depletion-layer model of the electronic structure of semiconductor grain boundaries developed by Taylor, Odell, and Fan (Reference 5), the activation energy, E_A, for zero-bias conductance of a grain boundary can be written (Reference 2) as

$$E_A = \phi_{B0} - T \frac{\partial \phi_{B0}}{\partial T} \tag{1}$$

where ϕ_{B0} is the potential barrier height at the boundary and T is the temperature. The potential barrier is created by the presence of excess charge at the boundary, because of majority carrier trapping. Its height can be written as

$$\phi_{B0} = \frac{e^2 Q^2}{8 \epsilon_0 \epsilon N_A} \tag{2}$$

where e is the electronic charge, Q is the total excess number of charges per unit area at the boundary, N_A is the net acceptor concentration in the material nearby the boundary, ϵ_0 is the permittivity of free space, and ϵ is the dielectric constant of Si. N_A is the local net acceptor concentration near the boundary, which can differ from the value in the bulk. The present study has not been able to distinguish between the effect of Q on E_A and that of N_A. In any case, the data shown in Figure 1 reveal clearly that significant variation in activation energy for zero-bias conductance along the boundary does exist, even within a sample having about 1 mm^2 boundary area.

To illustrate further the variation in activation energy, these energies for nine samples cut sequentially from a part of a bicrystal wafer are plotted in Figure 2 as a function of the distance from the edge of the wafer. The top portion of Figure 2 is a sketch of the part of the wafer containing the grain boundary under study, where the dashed line is a twin boundary. The wafer was cut along the direction parallel to the vertical axis of the graph. The width of each sample was about 1.3 mm. Each datum point represents the activation energy in the sample having the segment of the boundary just above the point as indicated in the sketch. If the sample had two observable activation energies, only the higher activation energy was plotted. From the figure, it is clear that the activation energy varies significantly along the boundary. The data seem to indicate that the activation energies of samples cut from the material near the wafer's edge are higher than those of samples cut from the material far from the edge. In addition, there is a peak in activation energy at about 8 mm to 10 mm from the edge. This peak corresponds to the boundary segment, A, whose orientation is considerably different from other segments. However, significant variation in E_A was also observed in other segments of the boundary, e.g., the long segment at the left of segment A. These

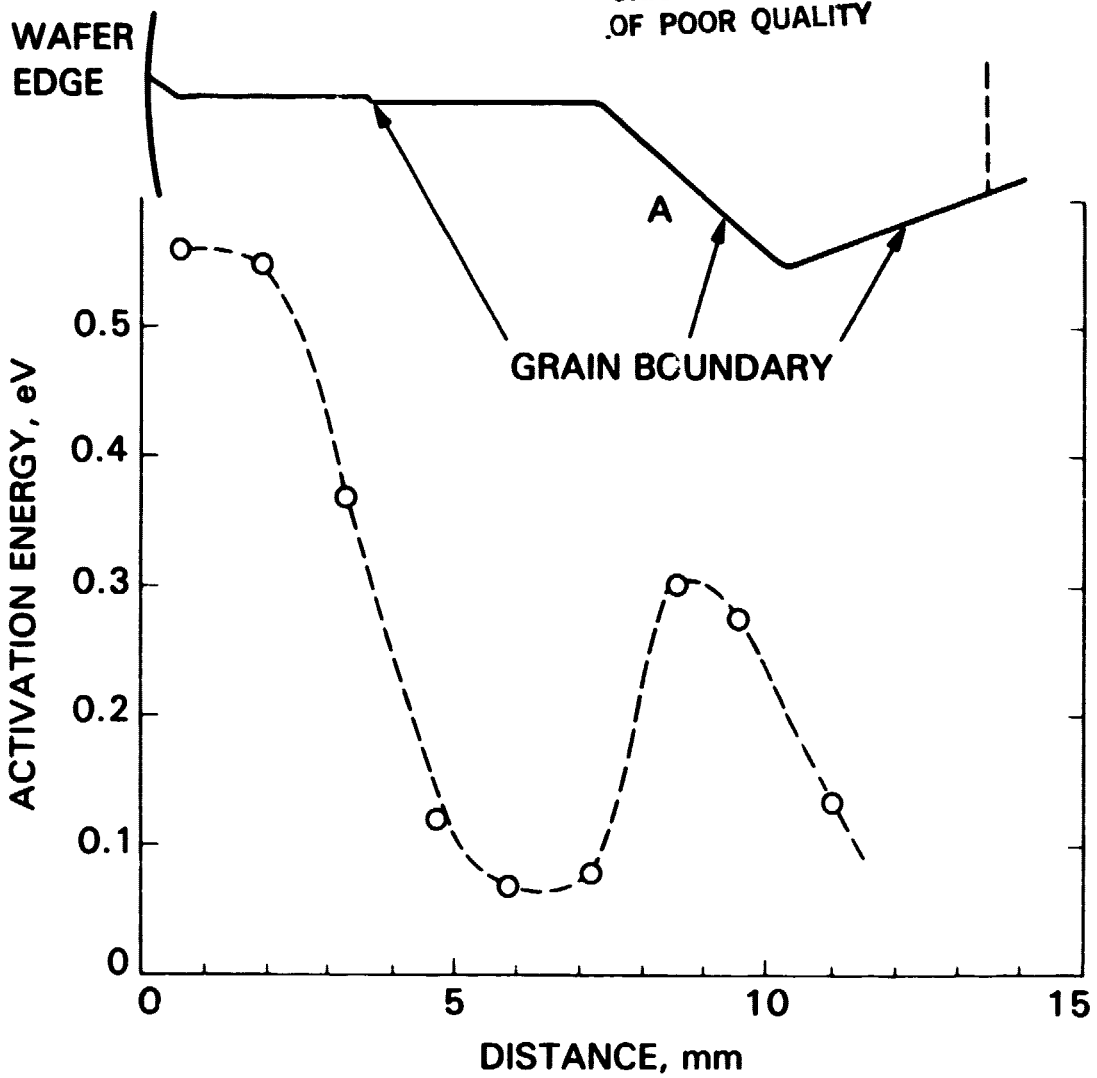

Figure 2. Activation Energies for the Temperature Dependence of Zero-Bias Conductance of Samples Cut From a Bicrystal Wafer, Plotted as a Function of the Distance From a Wafer Edge; Top Portion Represents a Part of a Wafer With the Grain Boundary Under Study

variations suggest that more studies are needed before any firm conclusion on orientation dependence can be made. At present, the variation can be attributed to the nonuniform distribution of intrinsic and extrinsic disorders along the boundary. The variation seems to depend on boundary orientation and some unknown parameters of crystal growth.

The effect of thermal treatments on grain-boundary properties is an important subject related to solar-cell applications of polycrystalline silicon. Several thermal treatments of bicrystals in hydrogen atmosphere were performed. Samples were treated at 550°C for 5 minutes for ohmic contact formation before any measurement could be made; thus, only the thermal effect after the metallization can be presented. Figure 3 illustrates the effects of isochronal annealing at temperatures of 600°C and 700°C on zero-bias conductance of a bicrystal sample. As indicated in the figure, the activation

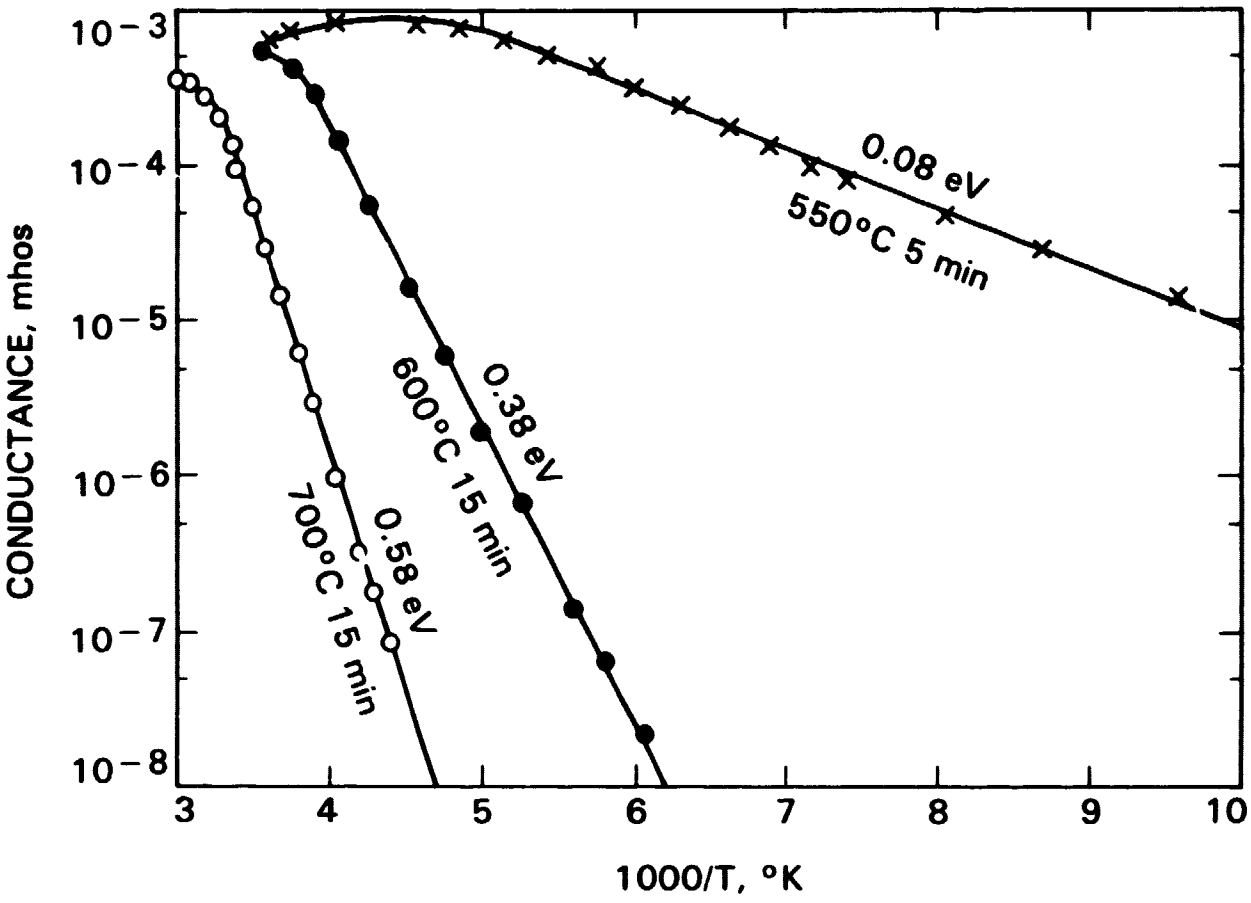

Figure 3. Effects of Isochronal Annealing at 600°C and 700°C on Zero-Bias Conductance of Bicrystal Sample

energy for the conduction process at the boundary was about 0.08 eV after the metallization. The value increased to 0.38 eV after a 15-min annealing at 600°C and to 0.58 eV after a sequential annealing at 700°C, as evident with the sharp decrease of the slope of the sample's conductance as the temperature decreases. The increase of the activation energy reflects the fact that the boundary becomes more capable of trapping majority carriers after annealing. This is consistent with the belief that the density of localized states of the boundary was increased after the annealing. This could be due to atomic rearrangement and/or impurity gettering at the boundary. For samples with activation energies around 0.55 eV, the thermal annealing at these two temperatures were minor. The detailed mechanisms involved in the thermal annealing processes are not known yet. Obviously, more studies are needed for better understanding of thermal treatment effects.

Since solar cells operate under illumination, it is important to know the effect of illumination on grain-boundary behavior. Figure 4 illustrates the illumination effect on the temperature dependence of the bicrystal samples. The light used was from an ELH lamp and its intensity was monitored using a standard solar cell. The light drastically reduced the temperature dependence

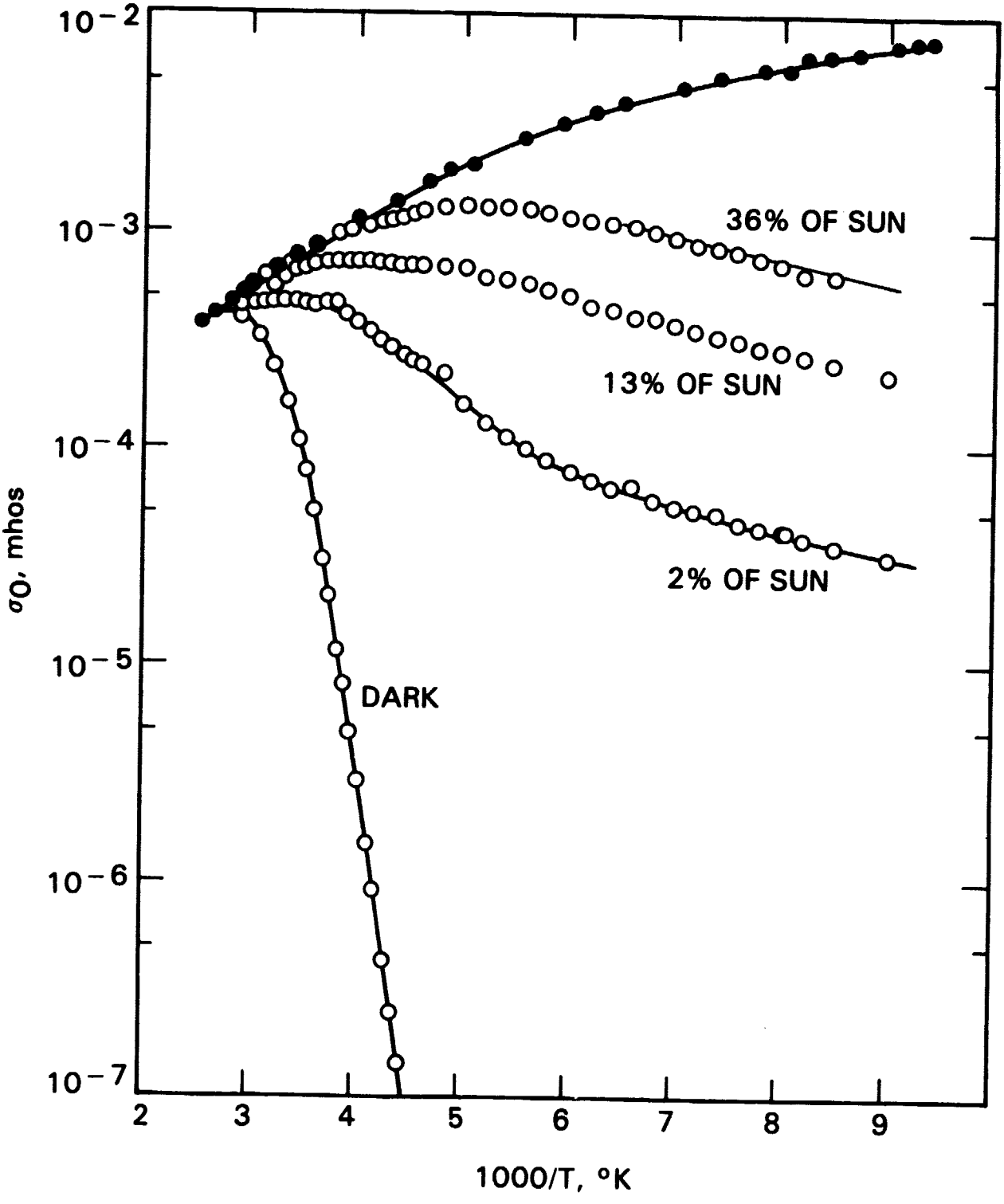

Figure 4. Effect of Illumination on Temperature Dependence of Bicrystal Sample

of the boundary conductance. As indicated by the data, a light of its intensity equivalent to about 30% of AM1 can effectively eliminate the boundary resistance. This suggests that a grain boundary existing parallel to cell surfaces may not have significant effects on the series resistance of solar cells.

D. CONCLUSIONS

Using temperature-dependence measurements of zero-bias conductance and deep-level transient spectroscopy, electrical properties of grain boundaries in p-type boron-doped bicrystal samples cut from silicon ingot grown by the Cz technique were studied. The results not only show the suitability of these two techniques for characterizing grain boundaries in silicon, but also provide new information concerning boundary properties. The experiment on the effect of illumination on the temperature dependence of boundary resistance suggests that a grain boundary parallel to the cell surface may not have significant effects on the series resistance of solar cells.

SECTION III

LOCALIZED STATES ASSOCIATED WITH GRAIN BOUNDARIES

A. INTRODUCTION

Electrical properties of grain boundaries in silicon, such as conductance (References 1 and 6), capacitance, barrier height, minority carrier lifetime (Reference 7), and recombination velocity (References 8 and 9) have been investigated. It is known that the electronic states in the energy band gap at the grain boundary due to the presence of structural defects actually dictate the electrical properties. Therefore, it is important to study the electronic states in the energy band gap at the grain boundary. One way to study the boundary states is to examine the transient behavior of the boundary capacitance of bicrystalline samples using DLTS (Reference 10). Previous results (References 6 and 9) have illustrated the applicability of the technique and revealed the continuous distribution of the density of states in the band gap.

The density of states at the grain boundaries was found to be a complicated function of the level location in the energy gap and the trapping cross sections. This complexity causes problems in data analysis using the simple method generally applied in DLTS studies. In addition, the electrical properties of a grain boundary were found to vary from sample to sample cut from the same bicrystal wafer (Reference 6).

This section reports experimental results concerning the electronic states at grain boundaries using DLTS, and a method of extracting the information from complex DLTS spectra. The results, including the observation of an anomalous pulse-repetition-rate-dependent DLTS signal, can be attributed to local variation of the defects in density and in type.

Subsection B offers results from samples cut from a boron-doped Cz ingot of nominal 30-ohm-cm resistivity, in which the growth directions in the bicrystal were [221] rotated about 160 deg with respect to each other.

In addition, a model of the boundary including spatial nonuniform distribution of the density of states is given; it is consistent with observations. Anomalous pulse repetition rates and pulse-width dependences, which can be explained with the nonuniformity model, also have been observed.

Subsection C presents results concerning localized states in a sample with 20-deg symmetrical (100) tilt boundaries, and a computer-fitting technique that is capable of extracting the density of states of the grain boundary from the complicated DLTS spectra is described.

B. FIRST EXPERIMENTS

The first group of experiments resulted in a method of extracting information from complex DLTS spectra and in the development of a modified double-depletion-layer model that is proposed to accommodate the nonuniform distribution of defects along the grain boundary.

1. Model

According to the double-depletion-layer model developed by Taylor, Odell, and Fan (Reference 5), the energy bands of a p-type silicon bicrystal are bent downward with a barrier height ϕ_{B0} (subscript 0 indicating that the sample is under zero bias) due to the trapping of the majority carriers (hole) at the grain boundary. The total number of carriers Q_b (per unit area) trapped at the grain boundary is given by References 1, 2 and 13:

$$Q_b = \int_E N_t(E)\Big[1 - f(E)\Big]dE \tag{4}$$

where f(E) is the Fermi function and $N_t(E)$ is the density of states at the grain boundary. Q_b and ϕ_{B0} can be measured using a capacitance technique (References 4, 5 and 7) with the formulas

$$\phi_{B0} = e^2\epsilon_s N_A/8C^2 \tag{5}$$

$$Q_b = \epsilon_s N_A/C \tag{6}$$

where C (farad/area) is the grain boundary capacitance, ϵ_s ($\equiv \epsilon_0\epsilon$)is the permittivity of silicon and N_A is the acceptor concentration in the grain.

The above model assumes $N_t(E)$ to be uniform along the grain boundary. However, $N_t(E)$ may vary along the boundary plane, i.e., Q_b and ϕ_{B0} are functions of the position along the grain boundary, as evident in previous results (Reference 6). The variation of the local barrier height is illustrated in Figure 5. When a voltage is applied to a sample, most of the current (current direction perpendicular to the plane of the drawing) passes through the boundary area having lower ϕ_B, as illustrated at position A in the figure. As a result of the charge trapping process occurring at position A, the local ϕ_B becomes larger (downward in Figure 5), and the local current becomes smaller. Consequently, the probability of the additional carriers being trapped in position A is reduced. However, the current through position B, which has higher ϕ_B, is originally less, so the change in ϕ_B is also less. The local difference in the change rate in Q_b and ϕ_B can cause unusual variation in DLTS spectra under different measuring conditions.

This local-barrier-height concept has not previously been exploited in grain boundary studies. The experimental results presented later in this paper strongly support this idea, which is more realistic than the simple model discussed in Reference 5.

2. Experiment

Samples were cut from a Czochralski-grown boron-doped silicon bicrystalline ingot of nominal 30 ohm-cm resistivity. The growth directions in the bicrystal were [221], rotated about 160 deg with respect to each other.

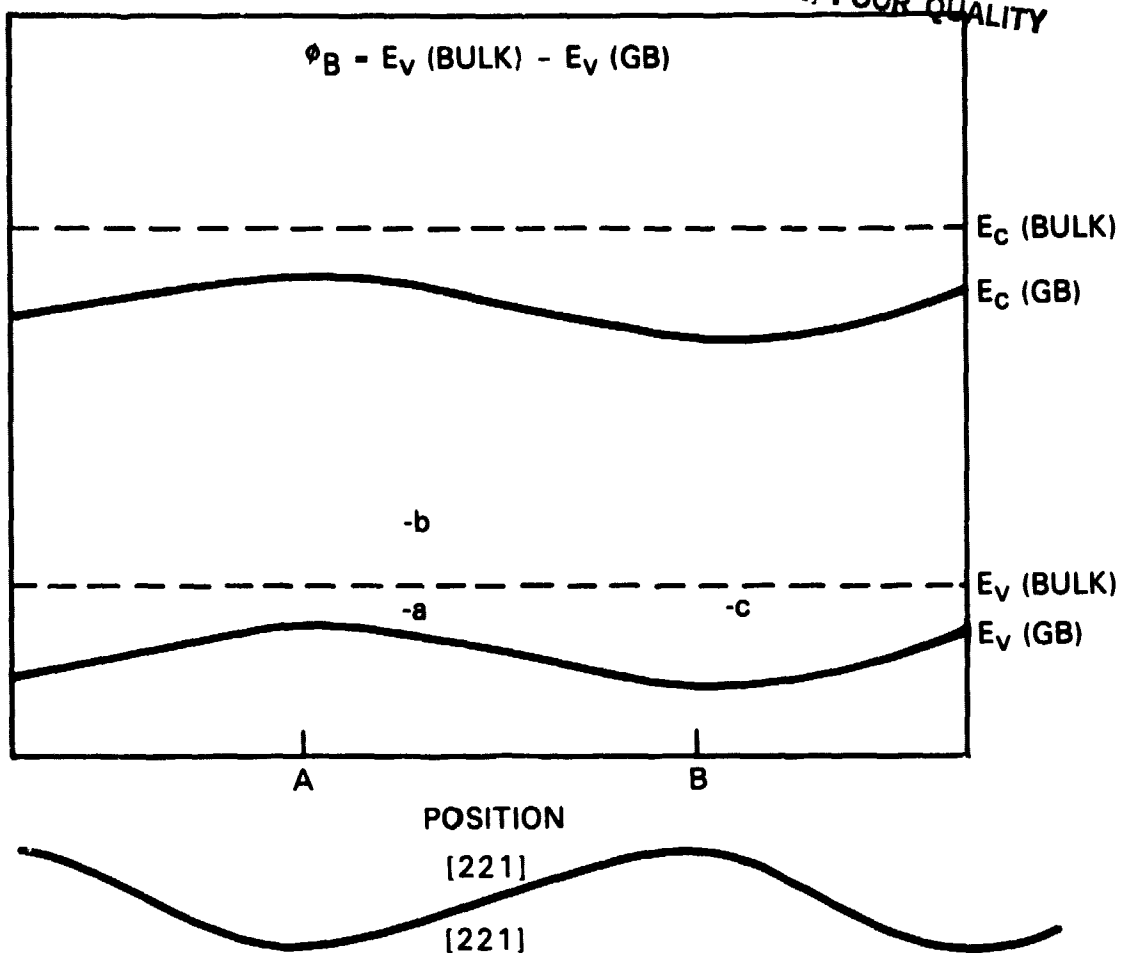

Figure 5. Variation of Barrier Height Along the Grain Boundary (GB)

The boundary plane is roughly parallel to a (114) plane of one crystal. However, the local boundary orientation varies considerably along the boundary plane and has not been determined for each sample. The ingot was first sliced into wafers along the direction perpendicular to the growth direction. The wafer was cut into bar-shaped samples with the grain boundary running across each sample. Two ohmic contacts were made on each side of the boundary by aluminum evaporation followed by sintering. After the contacts were made, the middle portion of the sample including the grain boundary was etched to eliminate undesirable surface effects.

The DLTS measuring system consists of a Boonton 72BD 1-MHz capacitance meter, an electronic gate, a pulse generator, a PAR 162 boxcar averager with two 165 gated integrators and an X-Y recorder. During the measurements the sample was mounted in a variable-temperature cryostat.

Since the equivalent circuit of a bicrystal consists of a boundary capacitance in parallel with a boundary resistance, then in series with a series resistance that is due to the grain material, a correction of measured capacitance is usually needed. The correction becomes more important at high temperatures; the boundary resistance decreases rapidly with increasing temperature. When the boundary resistance is much lower than the impedance of

the capacitance, the DLTS method becomes inapplicable. Figure 6 illustrates the difference between the measured and corrected DLTS signals, showing that the correction is important at high temperatures.

3. Results and Discussion

a. Repetition-Rate Dependence. Figure 7 shows two DLTS spectra measured with different repetition rates. The figure illustrates that the DLTS signal is reduced with the increase of repetition rate, but the signal at high temperature is roughly constant. This anomalous phenomenon cannot be explained by the usual grain-boundary model concerning uniform distribution of the defects. However, it can be explained in terms of the local barrier variation as discussed in Subsection III.B.1. For simplicity, only three levels are shown in Figure 5. It is assumed that the carrier emission from the shallow level (a) is responsible for the DLTS signal shown in the low-temperature region of the spectrum, and the carrier emission from the deep levels (b) and (c) are responsible for that in the high-temperature region. At a low repetition rate, almost all of the trapped carriers in both shallow and deep levels can escape in the low-temperature region. When the repetition rate is increased, the carriers trapped at level (b) do not have enough time to escape from the level between pulses at the low temperature where the signal from level (a) is measured. The local barrier height at position A remains higher than that in the case of the low repetition rate and, as a consequence, less current passes through position A. Therefore, the probability of level (a) being filled decreases considerably and the DLTS signal is reduced accordingly. ϕ_B at position B does not alter: neither does the trapped carrier concentration at level (c). Therefore, the DLTS signal remains constant in the high-temperature region.

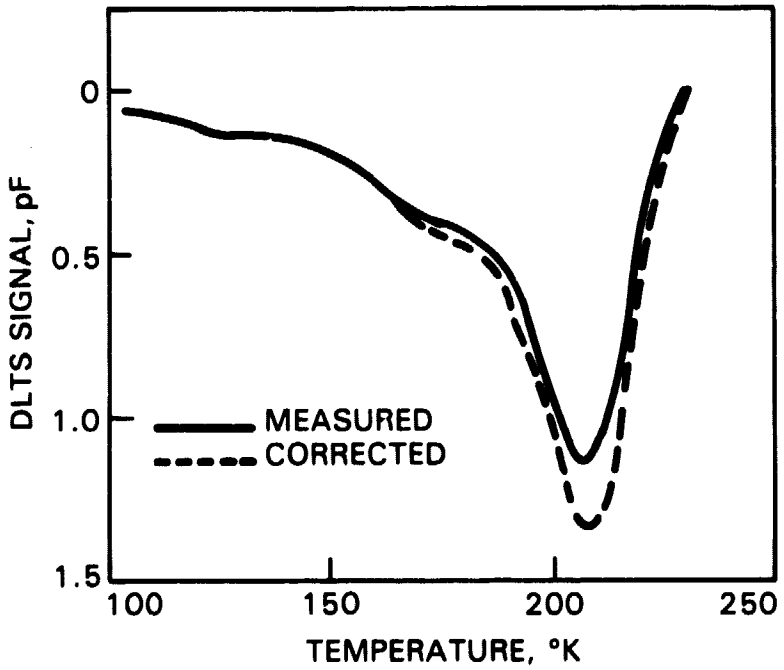

Figure 6. A Corrected and Measured DLTS Spectrum, Measured With 3-V Pulse Height, 10 μs Pulse Width, and 20/60 ms Gate Setting

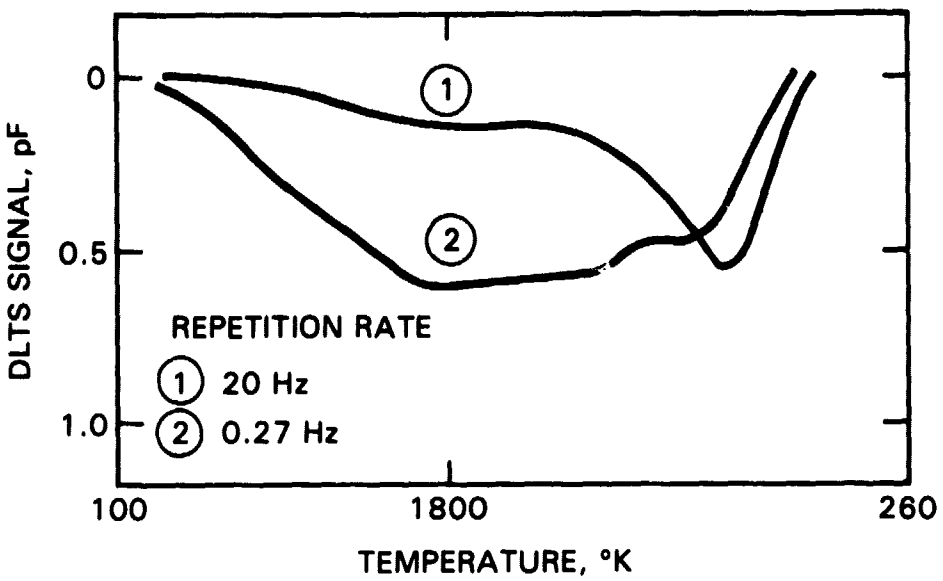

Figure 7. Repetition-Rate-Dependent DLTS Spectra, Measured With 4-V Pulse Height, 50 μs Pulse Width, and 10/30 ms Gate Setting

This explanation of the observed anomalous repetition-rate dependence is only a qualitative argument; detailed analysis of the rate dependence is still in progress. The DLTS technique is shown to be sensitive to the local spatial variation of the grain-boundary states.

b. Pulse-Width Dependence. Figure 8 shows a typical pulse-width dependence of DLTS spectra in a wide range covering a factor of 10^4, taken with 3 volts pulse height and 27.5/s rate window. The spectrum with a 1 μs pulse width has one peak (around 130°K) corresponding to a maximum in the distribution of the density of states at E_v + 0.17 eV and another broad peak (around 190°K) corresponding to states located at a deeper energy level in the band gap. The first peak (E_v + 0.17 eV) showed no significant increase with pulse-width increase. However, not only has the magnitude of the second peak been increased sharply with increasing pulse width, but also the peak position has been shifted toward a higher temperature. These changes can be attributed to the observed additional states that have smaller trapping cross sections or are at locations with different local barrier heights. The shift of the peak toward a higher temperature indicates that the additional states may be situated deeper in the energy band gap. The results suggest that the shallower levels are more easily filled than the deeper levels, implying that there are no strong interactions between shallow and deep states. This is consistent with the nonuniform distribution of defects, as described by the model.

c. Energy Level in the Gap at the Boundary. The method of estimating the separable energy levels using DLTS has been discussed by D.V. Lang (Reference 10). In this case, the capacitance transient decays exponentially and the DLTS peaks usually have the same magnitude as measured

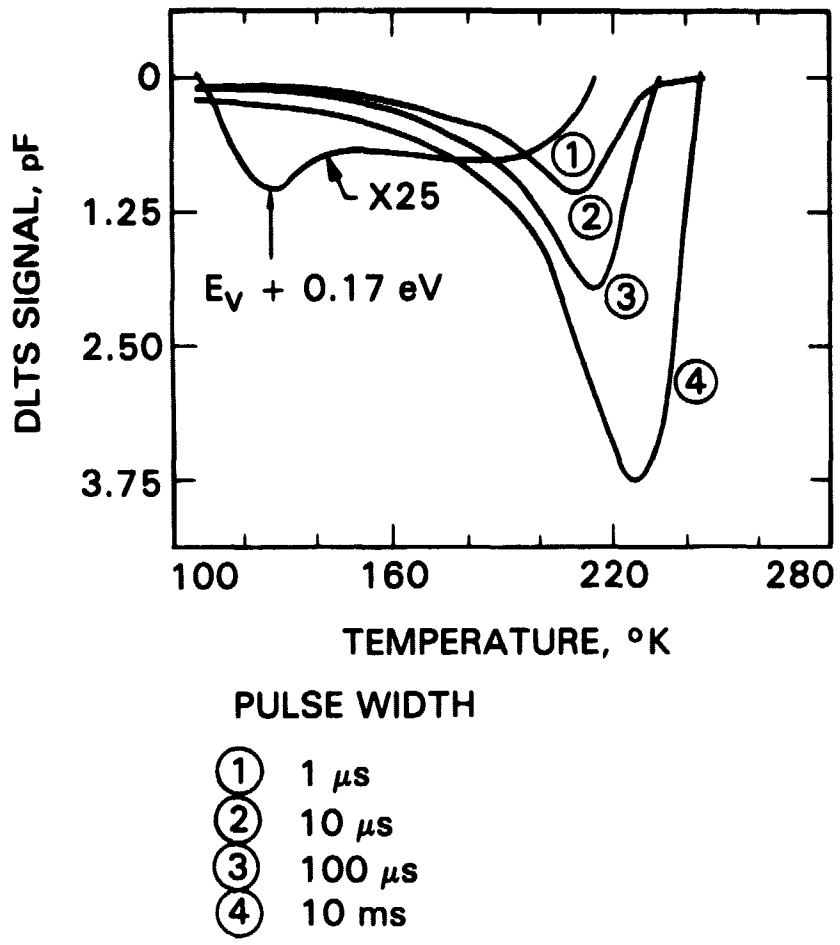

Figure 8. Pulse-Width-Dependent DLTS Spectra, Measured With 3-V Pulse Height, 20/60 ms Gate Setting and 1 μs, 10 μs, 100 μs and 10 ms Pulse Width for Curves 1, 2, 3 and 4, Respectively

with different rate window settings. However, this is not true for nonseparable levels such as those at grain boundaries, because the capacitance transient is the sum of many exponential decays. The expression for the DLTS signals for nonseparable levels can be obtained by extending Lang's method and can be expressed as

$$S(T) = \sum_i C_i(0) \left[\exp\left(-t_1/\tau_i\right) - \exp\left(-t_2/\tau_i\right)\right| \qquad (7)$$

where

T is temperature

$C_i(0)$ is the capacitance change due to level i just at the end of the pulse (i.e., t = 0)

$1/\tau_i$ is the emission rate for level i

t_1 and t_2 are the gate settings.

$C_i(0)$ and τ_i are functions of level characteristics, which makes the data analysis difficult. However, the difference of the DLTS spectrum due to the increase of pulse width (referred as a "difference DLTS spectrum") can be used to estimate the energy level, if the difference is mainly due to states situated roughly around one energy level. Then the amplitude of the difference DLTS spectra with different rate window settings can be equal, so Lang's method can be applied.

The experimental results show that the capacitance decay at the grain boundary is usually exponential when the pulse width is short, as shown in Figure 9(a), where the peaks of spectra measured with a constant 1 μs pulse width have the same amplitude. This implies that the transients are exponential and the energy level is found to be at E_v + 0.38 eV. Figure 9(b) shows similar spectra taken with a pulse width of 10 μs. The considerable difference in the magnitude of the peaks shows that the decay is not exponential and cannot be analyzed using Lang's method directly. However, the difference DLTS spectra have the same amplitude of peaks as shown in Figure 9(c); therefore Lang's method can be applied, which gives E_v + 0.48 eV as the energy of the level in the gap.

C. SECOND EXPERIMENTS

The new experimental results on the sample with 20-deg symmetrical (100) tilt boundaries made possible a detailed calculation of the density of states at the boundary.

1. Experimental Procedures

The sample was prepared from a 4.3 Ω-cm Cz-grown p-type bicrystalline silicon wafer with a 20-deg symmetrical (100) tilt boundary. The bar-shaped sample had two ohmic contacts on each grain with the boundary running across the middle of the sample. The details of the sample preparation and the experimental procedures have been described (References 6 and 11).

2. Results and Discussion

a. Zero-Bias Resistance and Capacitance Measurements. The purpose of the measurement is to determine the activation energy of the carrier transport at the boundary. In order to measure the value at a condition close to thermal equilibrium, the voltage across the sample was made much smaller than q/kT. Five mV were applied across the sample in the temperature range from 100°K to 400°K where q/kT is between 9 mV and 35 mV. Figure 10 is a typical plot of resistance as a function of temperature measured on the bicrystalline and single-crystalline silicon samples, respectively. According to thermionic emission theory, the boundary

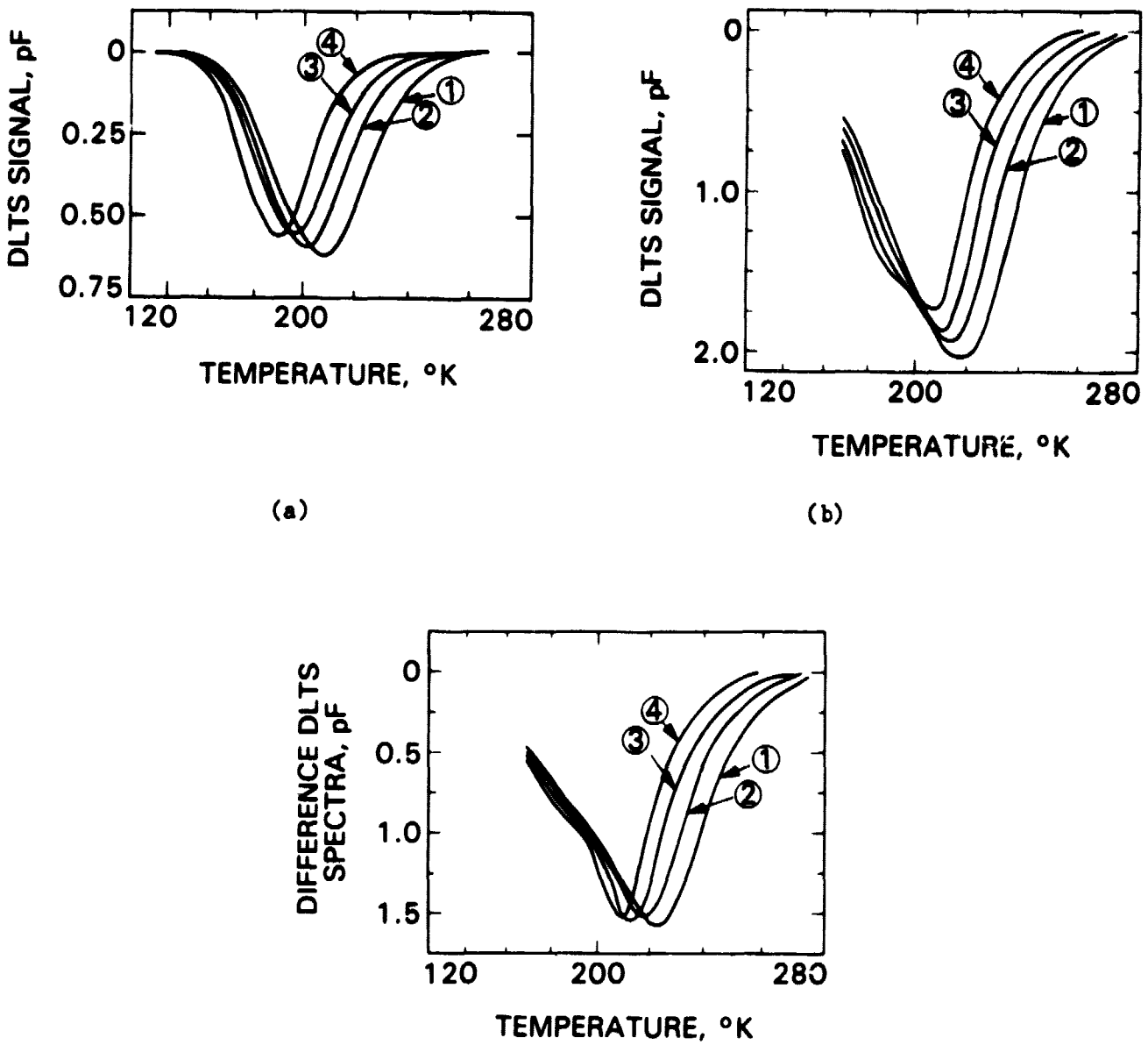

Figure 9. Gate-Setting-Dependent DLTS Spectra, Measured With 3-V Pulse Height, 5/15, 10/30, 20/60 and 40/120 ms Gate Settings for Curves 1, 2, 3 and 4, Respectively, and (a) 1 μs Pulse Width, (b) 10 μs Pulse Width, and (c) the Difference Between (b) and (a)

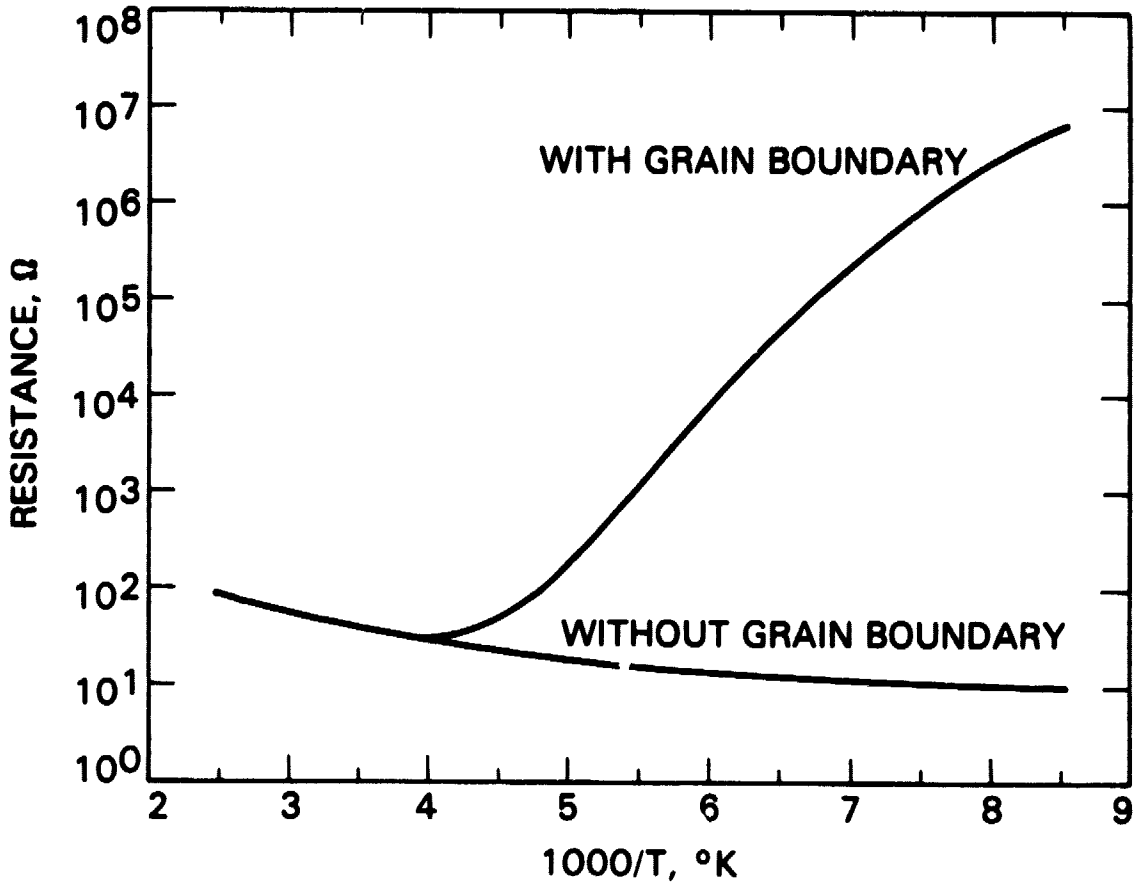

Figure 10. Temperature Dependence of Zero-Bias Resistance of Bicrystal and Single-Crystal Silicon Samples

resistance is an exponential function of the reciprocal of the temperature. At low temperatures, the resistance of the sample with the grain boundary is much larger than the bulk resistance, as shown in the diagram. As the temperature increases, the resistance of the sample with the boundary decreases drastically, as predicted by the theory, and the bulk resistance increases due to the decrease in mobility. At high temperatures, therefore, the bulk resistance and the bicrystal resistance are similar because the bulk resistance predominates.

After applying temperature correction, an activation energy of 0.30 ± 0.01 eV was obtained from the slope of the straight portion of a plot of $\ln(R)$ versus 1000/T, where R is the boundary resistance. The slope of the curve decreases gradually at low temperature. This indicates that some areas of the boundary plane have considerably lower activation energies and that the barrier height at the boundary is not uniform. In addition, it was found that the temperature dependence of boundary resistance is the same for all samples

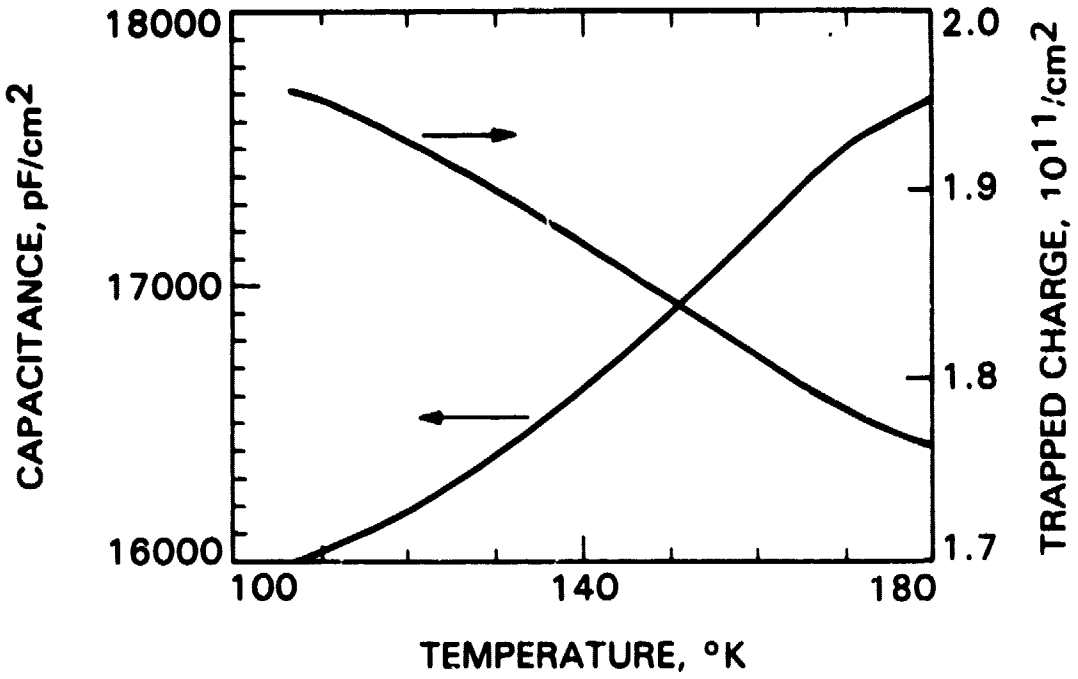

Figure 11. Measured Capacitance and Calculated Trapped-Charge Density at the Grain Boundary as a Function of Temperature

cut from a wafer, indicating that the nonuniformity occurs at a scale much smaller than the sample size.

Figure 11 shows the boundary capacitance, $C(pF/cm^2)$, as a function of temperature. The increase of the boundary capacitance with temperature indicates that the number of carriers, $Q_b(1/cm^2)$, trapped at the boundary decreases gradually with increasing temperature. Q_b is calculated from the measured values of capacitance by

$$Q_b = \epsilon_s N_A / C \tag{8}$$

where ϵ_s is the permittivity of silicon and N_A is the acceptor concentration in the grain. Q_b versus temperature is also shown in Figure 11. The result indicates that the distribution of the localized states at the boundary is continuous throughout the energy band gap, because of the smoothness of the curve.

b. Transient Capacitance Measurement. A boundary can be considered as two opposing Schottky diodes in series. The boundary states are assumed to be located between the Schottky barriers. A flow of current through the boundary is required for the DLTS measurement of the density of states at the boundary. The local current density through the boundary can vary strongly if the local barrier height varies, depending on the spatial distribution of the density of states.

In the non-uniformity model of the grain boundary used, which was supported by experimental data (Reference 11), the potential barrier can vary from place to place. Therefore, the current flowing through the boundary may not be uniform during the electrical pulsing of the DLTS measurement. The portions of the boundary with lower barrier height have higher current density and more carriers are available to become trapped. As a result of trapping, the local potential barrier becomes higher, and more current will flow through the portions of the boundary originally having a higher barrier. As a result of current flow in these portions, the states at these areas become more observable under DLTS measurement; i.e., the current will first fill the empty states at the grain boundary where the barrier is lower, and then will fill the states situated where the barrier is higher.

Figure 12 shows a typical pulse-width dependence of the DLTS signals of bicrystalline samples. On increasing the pulse width, the peak amplitudes increase and the peak positions shift toward a higher temperature. When the pulse width is narrow, the current fills only the shallower states situated in the low barrier height areas shown in Figure 12. As the pulse width increases, the states located in the area originally having a high barrier height will have a chance to be filled, and the DLTS signal due to these states becomes observable. These phenomena can be attributed to additional deep states situated where the barrier was originally higher and the local current density was smaller.

The pulse-width dependence of the DLTS measurements on bicrystal samples indicates that the shallower states are observed first. This suggests that there is no direct transition from the shallow level to the deep level; i.e., the boundary states are localized. It reveals that the physical distribution of boundary states is not uniform on a microscopic scale. This is consistent with the fact, generally known from defect studies on as-grown ingots, that the distribution of microdefects in silicon is always nonuniform (Reference 11).

c. Density of States at the Grain Boundary. The density of states at the grain boundary can, in principle, be obtained from the DLTS spectra, but the process is complicated, since the boundary states are continuously distributed in the energy band gap. The relationship between the DLTS signal S(T) and the density of states $N_t(E)$ at the grain boundary is approximated by

$$S(T) = \sum_{E} - (C_0^2/\epsilon_s N_A)\, N_t(E)\, \Delta E \left\{\exp\left[-r_E t_1 - \exp\left(-r_E t_2\right)\right]\right\} \qquad (9)$$

where C_0 is the boundary capacitance with the observed states being empty, r_E is the emission probability of the carrier at energy level E, t_1 and t_2 are the gate window settings, and the density of states is assumed to be a constant within a ΔE interval at an energy level E above the valence band edge E_v. The peak width of the DLTS spectra shown in Figure 10 is wider than that calculated for a single defect level, revealing the continuous nature of the density of states at the grain boundary. However, the width is not much larger than that for a single level. This indicates that the

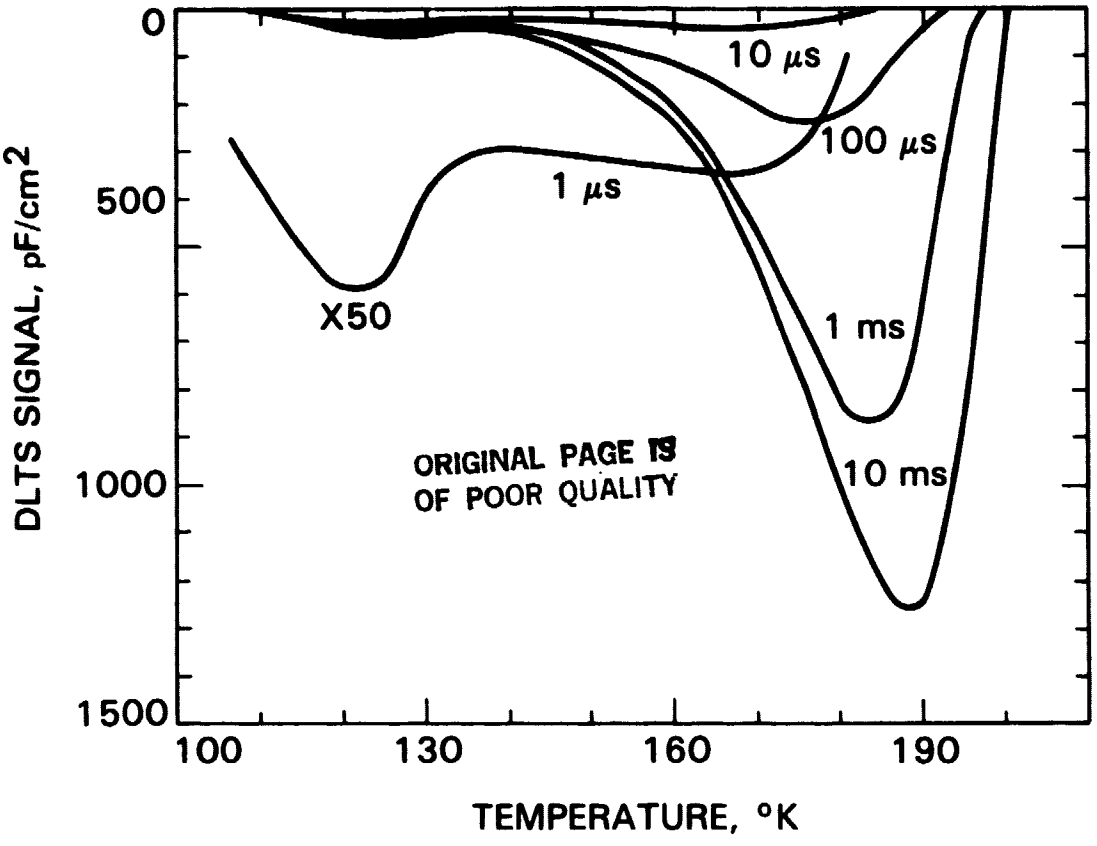

Figure 12. Pulse Width Dependence of DLTS Spectra; Measuring Conditions are 0 V Bias, 4 V Pulse Height, 20 ms and 60 ms Gate Window Setting

conventional technique can be used to estimate the position of the dominated state for the peak without introducing a considerable error. To verify this, r_E/T^2 versus 1000/T was plotted for several sets of data taken using different pulse widths. It was found that the data were always in the form of straight lines in this type of plot. Therefore, it can be assumed that the following formula is suitable for the grain boundary under study:

$$r_E = AT^2 \exp(-E/kT) \tag{10}$$

where A is a constant and depends on energy level. Figure 13 gives the experimental values of the A factor as a function of energy level. These A factors were obtained from a group of Arrhenius plots of the emission probability measured under various pulse-width conditions. The data seem to indicate that the A factor increases exponentially with energy level. To simplify the calculation of the density of states, it was further assumed that the relationship is appropriate for all the states observed. Then the density of states can be obtained using curve fitting of the DLTS data with the calculated curve using N(E) as a variable. The result of this curve fitting for the data shown in Figure 12 is shown in Figure 14. There are two groups

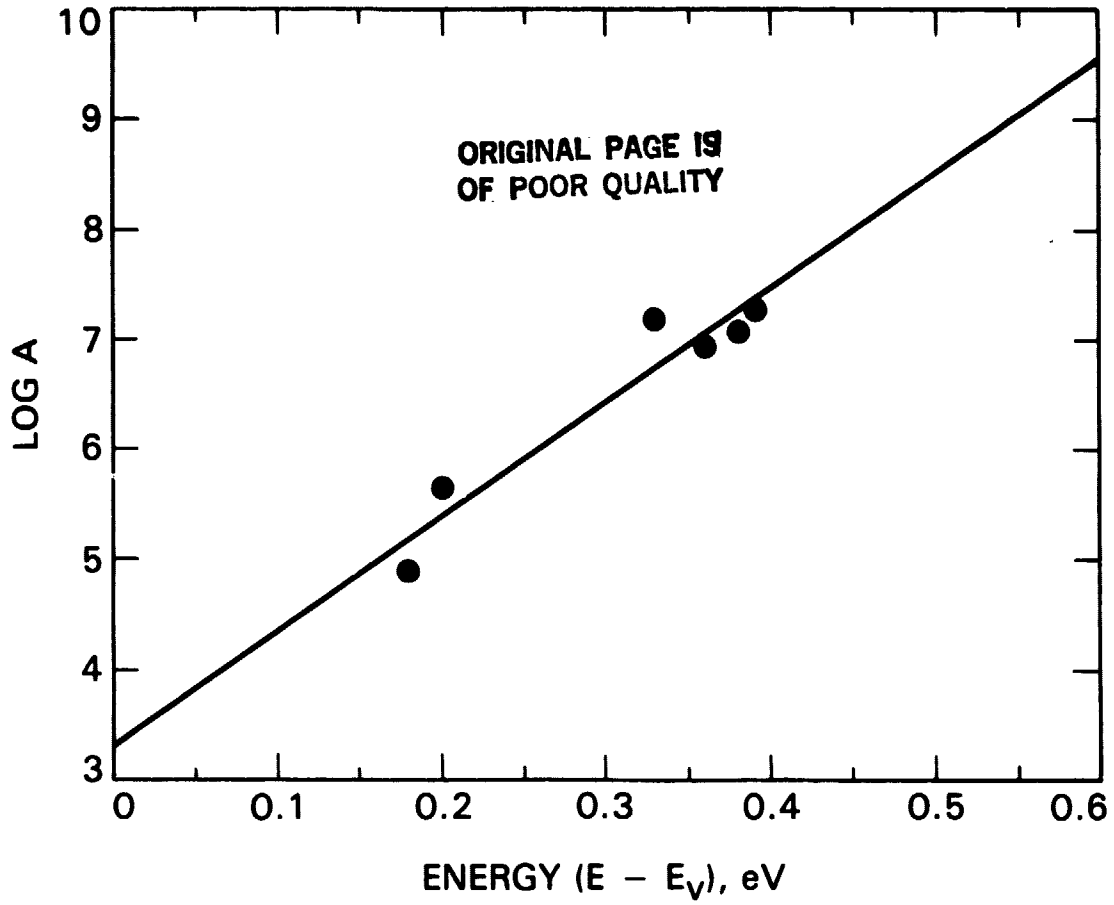

Figure 13. The Pre-Exponential Factor A of Emission Probability as a Function of the Energy Level Extracted From DLTS Data

of states clearly shown in the figure. A group of narrowly distributed states centered at E_V + 0.20 eV can be observed with short electrical filling pulses. The density of states of the other group, which was observed only with longer filling pulses, increases exponentially as the level becomes deeper. Because of the deterioration of the boundary capacitance at higher temperatures, only a part of this group was observed. The observation supports the common assumption that the density of states at the grain boundary increases exponentially as the state moves away from the band edge (Reference 12). However, the results from the study do showthe existence of noticeable deviations from the exponential dependence, such as the observation of the narrowly distributed states centered at E_V + 0.20 eV.

As noted above, Equation 10 is appropriate for use in the analysis of data observed in this study. Since the formula is similar to the one derived from the principle of the detailed balance, the analogy suggests that the A factor is proportional to the capture cross section. As a consequence, the data shown in Figure 13 indicate that the deeper levels have larger crosssections. This argument does not contradict the observed fact that the deeper levels were observed only with longer pulses, because the capture rate of each state is a product of the capture cross section and the local current density. In addition, the argument suggests that the local current density

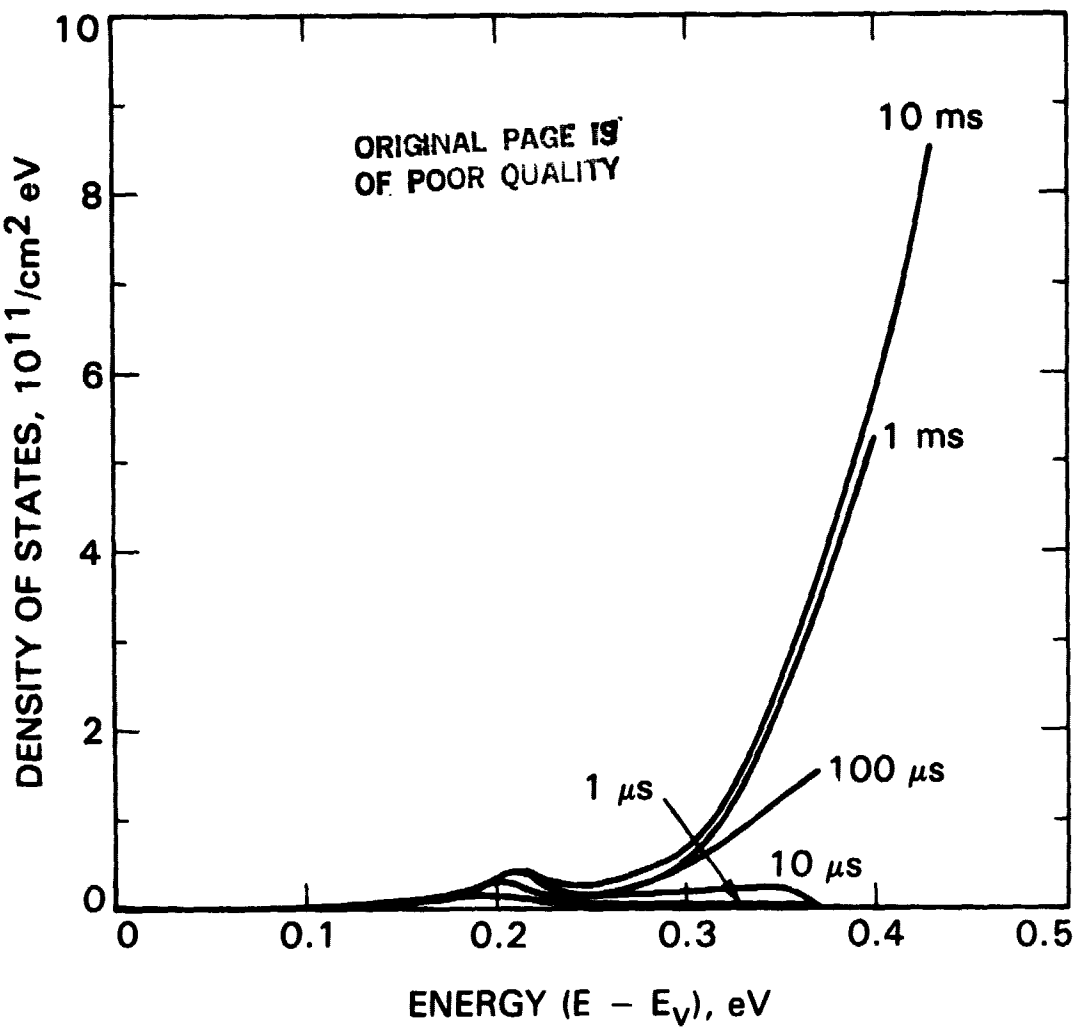

Figure 14. Density of States at Grain Boundary, Calculated From DLTS Spectra Shown in Figure 10

through the location of the deep level is small, i.e., the deep states are situated where the barrier height is higher. A conclusion from this argument is that the spatial distribution of the levels along the grain boundary may not be uniform.

The maximum density of states observed is about 9 x 10^{11}/cm^{2}eV under the 10-ms pulse-width condition (Figure 14). The maximum density of the states measured in the group of states centered at E_V + 0.20 eV is about 4 x 10^{10}/cm^{2}eV, which is considerably lower. The densities of states in the present samples are about 10 times larger than those in the previous samples (Reference 6), which could be attributed to the fact that the two studies were carried out on different boundaries. However, narrowly distributed states centered at E_V + 0.20 eV were found in both cases, indicating that they could result from the same kind of lattice defects at the boundary.

The total number of trapped carriers at the grain boundary is about 2 x 10^{11}/cm^2 at 105°K, estimated from the capacitance at thermal equilibrium

(Figure 11). This could represent the total density of states between the Fermi level at 105°K and the middle of the band gap, where the neutral level of the grain boundary is assumed to be. The integrated density of states under the curve of 10-ms pulse width in Figure 12 is about $6 \times 10^{10}/cm^2$ between the valence band and $E_v + 0.43$ eV. These results show that boundary states are mainly at deep levels in the gap. It should be noted that states deeper than those indicated in Figure 14 could not be observed because the barrier of the boundary deteriorates at higher temperatures.

SECTION IV

LIGHT EFFECTS ON GRAIN-BOUNDARY PROPERTIES IN SILICON

A. INTRODUCTION

The presence of a suitable flux of photons can modify grain boundary properties in semiconductors significantly. These light effects are especially important to the operation of photovoltaic devices. Card and Yang (Reference 7), Panayotatos and Card (Reference 12), Seager (Reference 13) and Fossum and Lindholm (Reference 14) have offered theoretical discussions on electronic processes, including recombination currents, at silicon grain boundaries under optical illumination. Only very limited experimental data are available, however, which makes any detailed understanding of the phenomena difficult. This section presents preliminary results of an experimental study of light effects on grain boundary properties in silicon, using measurements of photoconductivity (including kinetics), dark capacitance, and zero-bias conductance. The results not only provide important information concerning carrier transport phenomena at the grain boundary in silicon, but also offer an experimental method to measure the minority carrier recombination velocity at the boundary. Since the grain boundary is a planar defect, its photoconductive phenomena are considerably different from those in the bulk.

B. MODEL FOR GRAIN-BOUNDARY PHOTOCONDUCTIVITY

According to the commonly used double-depletion-layer model of the electronic structure of the grain boundary in semiconductors, developed by Taylor, Odell, and Fan (Reference 5), and modified by Pike and Seager (Reference 2), the electrical conductivity of a grain boundary under the zero-bias condition can be written as

$$G_0 = (eA/kT) \exp [-(E_f + \phi_{B0})/kT] \qquad (11)$$

where

E_f = the Fermi energy of the sample with respect to the edge of the majority carrier band

ϕ_{B0} = the height of the potential barrier at the boundary

e = electron charge

A = the Richardson constant

k = the Botzmann constant

T = temperature.

The zero-bias condition has been defined as an experimental condition in which the value of eV is much smaller than that of kT (Reference 2), where V is the voltage across the boundary. Experimental conditions were consistent with this zero-bias condition. Under illumination, G_0 changes as a result of the

change in the net charge density at the boundary due to a number of charge transport processes induced by the light. It is assumed that the light is uniformly absorbed through the sample. The time derivative of G_0 can be written as

$$d(G_0)/dt = -eA/(kT)^2 \exp\left[-(E_f + \ _{B0})/kT\right] d(\phi_{B0})/dt \tag{12}$$

$$= -(G_0/kT)\ d(\phi_{B0})/dt \tag{13}$$

At a fixed temperature, $_{B0}$ is the only variable that is related to the net charge density, Q (number of charges per unit area), at the boundary, and to the dopant density in the bulk, N_A, by the formula

$$\phi_{B0} = e^2Q^2/8\epsilon_0\epsilon N_A \tag{14}$$

where

ϵ_0 = permittivity of free space

ϵ = the dielectric constant of the semiconductor.

Except under high injection-level conditions, N_a is usually a very slow variable in comparison with Q. Therefore, N_a can be assumed to be a constant in the present work. Then,

$$d(\phi_{B0})/dt = (e^2Q/4\epsilon_0\epsilon N_A)\ d(Q)/dt \tag{15}$$

It is clear, from Equations 11, 12 and 15, that the photoconductivity of a grain boundary is mainly attributable to the light-induced change in Q.

There is a number of light-induced charge-transport processes that cause Q to change. Only those that are important to the present problem are considered. Trapping of the light-generated minority carriers starts at the moment the light is turned on because of the Coulomb attraction due to the trapped majority carriers, whose influence extends into the bulk by means of the depletion regions. The minority carrier trapping reduces the barrier height and, consequently, increases the majority carrier trapping. The combination of these two light-induced processes creates a new equilibrium condition in which Q is lower and a recombination current at the boundary is generated. The rate of change in Q during the transition period is equal to the difference between the net minority carrier trapping current, J_{min}, and the net majority carrier trapping current, J_{maj}, at the time. The latter is the difference between two processes, majority carrier trapping and thermal emission. In the above model the direct excitation processes of charges from the local states at the boundary to the carrier bands are ignored, since these processes are believed to be minimal. Furthermore, it is assumed that the emission of trapped minority carriers from the boundary is negligible, because the boundary usually has a net trapped majority carrier charge density that makes escape difficult. According to recent work by Seager (Reference 13),

J_{maj} can be written as $(2cA - B) \exp [-(E_f + \phi_{B0})/kTR$ and J_{min} as $(eD_e/L_e)\ (n_\infty - n_0)$, where B is the prefactor of the thermal emission process, c is the fraction of overbarrier majority carrier current that is captured at the grain boundary, D_e is the diffusion coefficient of minority carriers, L_e is the diffusion length of minority carriers, n_∞ is the photogenerated minority carrier density in the bulk far from the boundary, and n_0 is the same at the depletion region edge.

The above model has used a simplification by assigning the same trap parameters to all of the localized grain-boundary states. As shown by the experimental results from DLTS studies (References 6 and 15), the density of states at the boundary not only is a function of energy position in the gap, but also is a function of trapping cross-section. In addition, the experimental data also show that the density of states can vary with position, due to variations in defect type and concentration along the boundary. For practical purposes, these localized effects are not considered in this study. The conductance and the barrier height, however, are macroscopic properties that usually are not very sensitive to the details of the microscopic nature of localized states at the boundary. Therefore, the above- mentioned model is adopted to analyze the photoconductivity data without too much ambiguity. Then the kinetic equation for Q is

$$ed(Q)/dt = (2cA - B) \exp \left[-(E_f + \phi_{B0})/kT\right] - (eD_e/L_e)\ (n_\infty - n_0) \qquad (16)$$

under illumination and

$$ed(Q)/dt = (2cA - B) \exp \left[-(E_f + \phi_{B0})/kT\right] \qquad (17)$$

in darkness.

The recombination velocity at the grain boundary is of interest to many workers in the field of polycrystalline semiconductors. At equilibrium with light, the recombination velocity, S, at the boundary can be estimated using:

$$S = J_{min}/en_0 \qquad (18)$$

This formula is used below to estimate the recombination velocity at different boundaries, and its light-intensity dependence (Reference 13).

C. EXPERIMENTAL DETAILS AND DATA ANALYSIS

Samples were boron-doped p-type silicon bicrystals of nominal 30 ohm-cm resistivity. The detailed characteristics of the samples were described in Reference 6, which also provides the details of the zero-bias conductivity measurement.

The photoconductivity measuring system consisted of a 1.06-μm light-emitting diode with rise and fall times of about 10 ns, a constant-voltage supply for the bias, a light-tight enclosed box accommodating the sample and the light-emitting diode, a Systron-Donner Model 110B pulse generator, a PAR Model 115 wide-band preamplifier, a PAR Model 165 boxcar averager with a PAR Model 163 sample integrator, and an X-Y recorder. The voltage across the boundary was always kept at a value of $\leq$5 mV to ensure that the measured value would represent a reasonable value under the zero-bias condition. All of the photoconductivity measurements were made at 300°K. To examine the net charge trapped at the boundary, a HP Model 4271 1-MHz LCR meter was used to measure the capacitance and the conductance of the boundary C(D) and $G_0(D)$. The measured capacitance gives the net charge density, Q(D), and the barrier height, $\phi_{B0}(D)$ by means of the formulas

$$Q(D) = \epsilon_0 \epsilon N_a / C(D) \tag{19}$$

$$\phi_{B0}(D) = e^2 \epsilon_0 \epsilon N_a / 8C(D)^2 \tag{20}$$

Since G_0 is proportional to exp $[-(E_f + \phi_{B0})/kT]$, the zero-bias conductivity of the boundary at equilibrium with light intensity I can be written as:

$$G_0(I) = G_0(D) \exp \left\{-[\phi_{B0}(D) - \phi_{B0}(I)]/kT\right\} \tag{21}$$

With known experimental values of $G_0(I)$, $G_0(D)$, and $\phi_{B0}(D)$, the value of $\phi_{B0}(I)$ can be calculated. Using Equation 13, the value of Q(I) can also be obtained. The photoconductivity kinetics measurement can give Q(I) as a function of time. Similarly, the experiments can provide Q as a function of time during the recovery period in the dark.

Single-crystal samples cut from the same ingot were also examined, using photoconductivity and conductance measurements for material properties. The majority carrier density in the material was estimated at $5 \times 10^{14}/cm^3$, based on the conductivity measurement. The minority carrier lifetime was measured at about 10 μs, which gives the value of the minority carrier diffusion length as 1.84×10^{-2}cm. The single-crystal sample was used as a light-intensity monitor and the measurement gave the minority carrier density n_∞ in the bulk far from the grain boundary, which is needed for the estimation of the recombination velocity. It should be noted that the photoresponse in the bulk is found to be at least one order of magnitude smaller than that at the grain boundary.

D. EXPERIMENTAL RESULTS AND DISCUSSION

As shown in Equations 12 and 13, the rate of change in grain boundary conductivity due to illumination is not related to the rate of the change in the charge trapped at the boundary in a simple way. To present photoconductivity data in a meaningful way, they must be converted into the

form of Q as functions of time and other parameters using Equations 14 and 21. Table 1 lists some electrical properties of two grain boundaries of different barrier heights at room temperature. These two grain boundaries are considered to be representive of the present study. Sample No. 51 has a reasonably high thermal activation energy of 0.55 eV for the zero-bias conductance; the activation energy of sample No. 59 is only 0.1 eV. From the measured capacitance per unit area, the barrier height ϕ_{B0}, and the net charge density Q can be estimated using Equations 19 and 20.

Table 1. Electrical Properties of Grain Boundaries

Sample No.	E_a, eV	G_0, mho/cm^2	ϕ_{B0}, eV	Q (/cm^2)	I*	S, cm/s
51	0.55	0.0598	0.12	5.66×10^{10}	0.66 I	250
					I	640
59	0.10	0.245	0.02	2.22×10^{10}	I	88
					1.8 I	109

*I = Light intensity that creates an equilibrium minority carrier density of 1.08×10^{12} electrons/cm^3 in the bulk of the sample.

Figure 15 shows the time variation of Q at the grain boundary of sample No. 51, starting from the time the light-emitting diode is turned on. The intensity of the light I as measured by the sample is that which is capable of creating an equilibrium minority carrier density of 1.08×10^{18} electrons/cm^3. The rate of the change becomes slower and slower with time, and finally Q reaches an equilibrium value of 4.11×10^{10}/cm^2 after 3 or 4 ms. The initial value of the rate of change was estimated at 8.8×10^{10}/cm^{2}s. Figure 16 shows the recovery of Q at the boundary of sample No. 51 after the light was turned off. The initial rate of recovery was estimated at 6.35×10^{14}/cm^{2}s. The complete recovery of Q in this sample took more than 20 ms. Figure 17 gives the decay and the recovery of Q at the grain boundary of sample No. 59 under the same illumination condition. The initial rate of decay due to illumination, and of the recovery in darkness, were estimated at 1.41×10^{12}/cm^{2}s and 9.1×10^{13}/cm^{2}s, respectively. The data in Figure 17 show that the times required to reach the equilibrium conditions under illumination and in darkness are significantly shorter than those of sample No. 51 (Figures 15 and 16). This is consistent with the fact that the grain boundary in sample No. 59 has a smaller barrier height compared with that in sample No. 51.

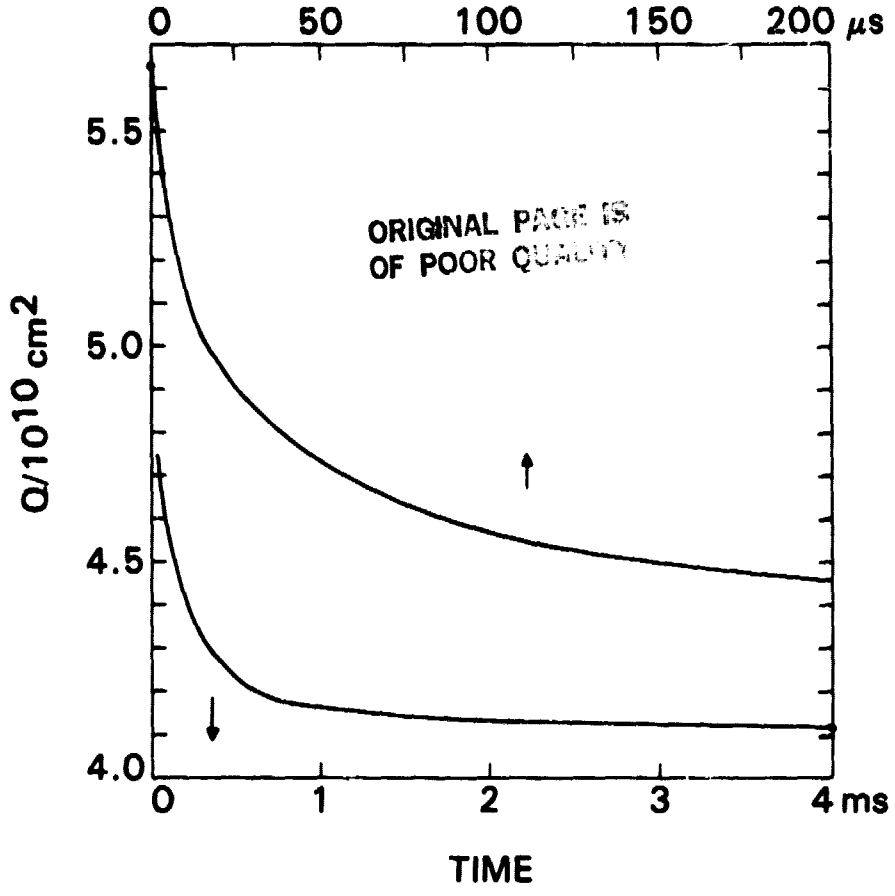

Figure 15. Decrease of Q Under Illumination, Sample No. 51

When Q reaches the equilibrium value under illumination, J_{maj} is equal to J_{min}, i.e.,

$$(2cA - B) \exp [-(E_f + \phi_{B0})/kT] = eD_e/L_e(n_\infty - n_0) \qquad (22)$$

from Equation 16. The product of the electron charge and the initial rate of the recovery of Q in darkness should be equal to the left side of Equation 22, as shown by Equation 17. Using the experimental values of L_e (1.84×10^{-2} cm), D_e (34 cm^2s), and n (from single-crystal sample measurements), one can estimate the value of n_0 by means of Equation 22. Then, using Equation 18, the minority carrier recombination velocities at the grain boundary under illumination can by estimated. Table 1 shows the calculated values of the minority carrier recombination velocity at the grain boundaries in samples No. 51 and No. 59 under different light intensity. The result reveals two important features: S increases with Q and ϕ_{B0}, as expected, since they all should be proportional to the density of states at the grain boundary; the value of S is also found to increase with light intensity. This observation is also understandable, because the illumination lowers the barrier height as a result of minority carrier trapping and, consequently, increases the recombination

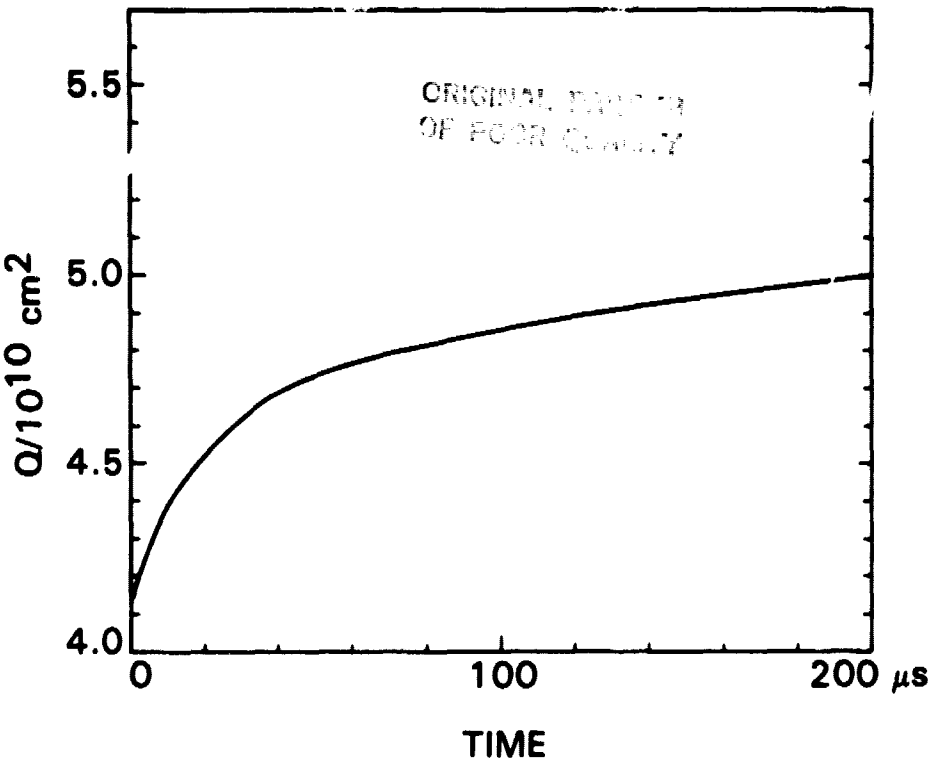

Figure 16. Recovery of Q in Darkness, Sample No. 51

velocity. Since the barrier height of the boundary in sample No. 59 in darkness is very low, about 0.02 eV, the effect of light on it is not expected to be substantial; no significant increase in S was observed. It is expected that the value of S at any grain boundary becomes saturated when the boundary is exposed to a very strong light.

These observations are consistent with the theoretical calculation of the recombination velocity at the grain boundary in silicon by Panayotatos and Card (Reference 12), which shows that S increases with minority carrier concentration. However, the theoretical calculation of Seager (Reference 13) indicates that S decreases with the generation rate. At this writing, the authors have had no explanation for the discrepancy. Obviously, more theoretical and experimental work is needed to understand carrier transport phenomena at the grain boundary in semiconductors.

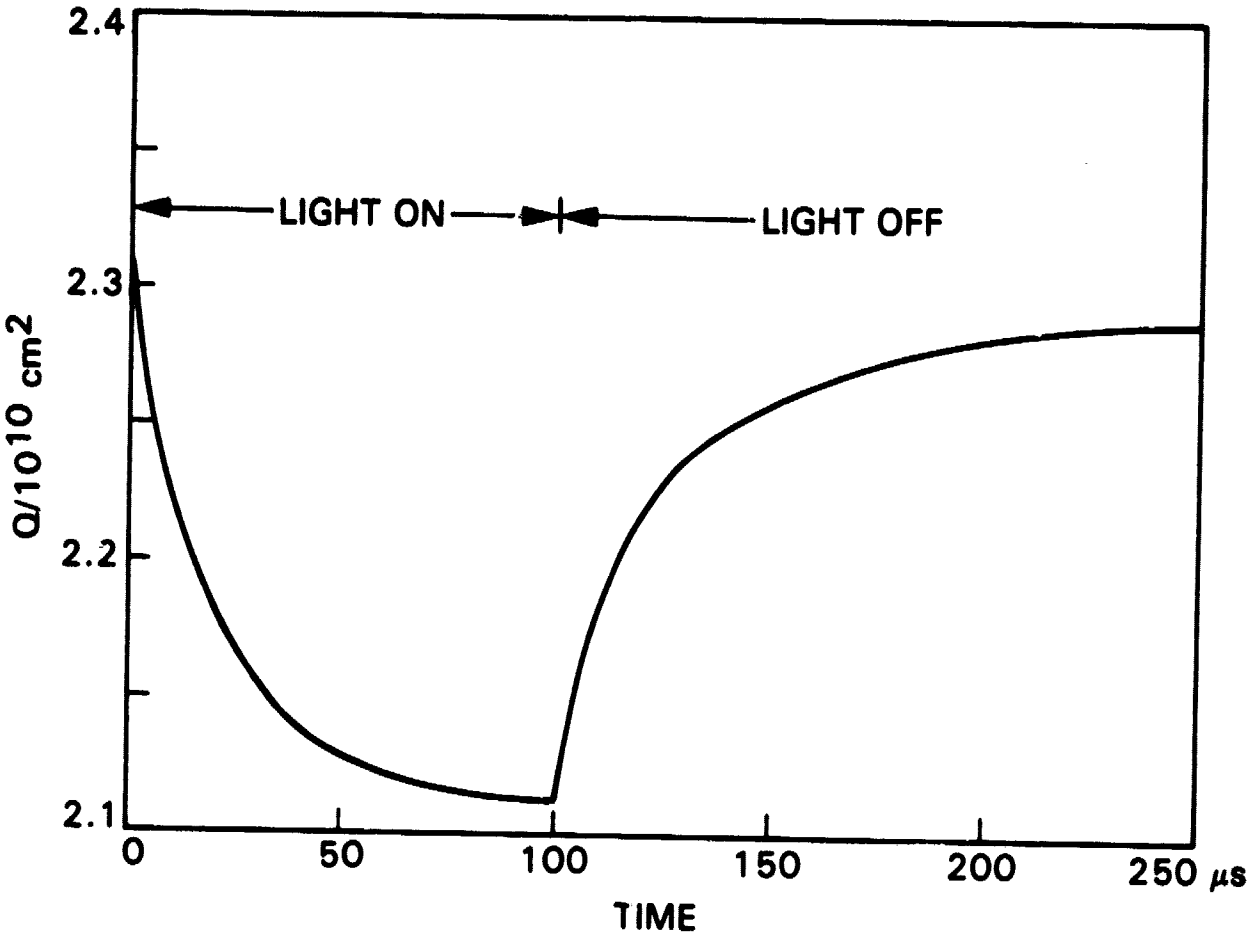

Figure 17. Light-Induced Change in Q and Its Recovery in Darkness

SECTION V

ENHANCED DIFFUSION OF PHOSPHORUS AT GRAIN BOUNDARIES

A. INTRODUCTION

Enhanced diffusion of phosphorus at grain boundaries in polycrystalline silicon materials has been considered to be a potential technique for the fabrication of more efficient polycrystalline solar cells (e.g., Reference 16). It was first discovered more than 20 years ago (Reference 17). It is believed that enhancement can increase the carrier collection area and reduce the recombination effect. Because of its complexity, only limited knowledge has been available on the detailed mechanism of the phenomenon, its relationship to material properties (particularly those of the grain boundaries) and its benefits in solar-cell applications.

In this section, results of a study on enhanced diffusion of phosphorus at grain boundaries in three cast polycrystalline photovoltaic materials (Wacker, HEM, and Semix) are reported. The study dealt with two concerns: the importance of enhanced diffusion to the efficiency under commonly used fabrication processes, and the relationship of enhanced diffusion to boundary structures.

B. EXPERIMENTAL DETAILS

The samples used were wafers of cast polycrystalline p-type silicon (Wacker, HEM, and Semix) supplied by the manufacturers for solar-cell applications. A set of samples was diffused at 850°C for 30 min, similar to the typical phosphorus diffusion process for solar-cell fabrication. Another set of samples, from Wacker wafers only, was diffused at 1100°C for 30 min. A grooving-and-staining technique (Reference 18) using concentrated hydrofluoric acid as a staining agent, was used to reveal the n-type diffused region, including enhanced diffusion at grain boundaries. Hydrofluoric acid can only stain p-type material, which makes n-type material show up as a bright region; consequently, the enhanced diffusion at grain boundaries manifests itself as white lines in a reflected-light photograph. Detailed features of stained sample surfaces were examined under a Zeiss metallurgical microscope. In order to assure that the white lines appearing beyond the bulk-diffused region were attributable to enhanced phosphorus diffusion at grain boundaries, a detailed comparison of the images of n-type material from the staining experiment and those of negatively charged phosphorus-silicon complex ions, obtained from an IMS-3F secondary ion mass spectroscope (SIMS), was made. EBIC images of a limited number of samples also were examined, using an ISI-60A scanning electron microscope to investigate the relationship between recombination activities and enhanced diffusion at grain boundaries. Sirtl etching was used to reveal the structural defects appearing at the surface, to examine those boundaries responsible for the enhancement.

C. EXPERIMENTAL RESULTS

Figure 18 shows a typical comparison between two images of a Wacker sample diffused at 1100°C: optical photographs of n-type diffusion region (bright region in Figure 18a), and a SIMS picture of negatively charged phosphorus-silicon complex ions. Figure 18a shows an image of two boundaries as white lines extended from the bulk diffused region, forming a triangular shape. Figure 18b shows the same line image of phosphorus ions taken by SIMS. The one-to-one correspondence between the two images assures that the white lines observed by the groove-and-stain technique is due to enhanced diffusion of phosphorus. The appearance of the sample after Sirtl etching, observed under an optical microscope, confirmed the existence of the boundaries. Figure 19 shows another Wacker sample, photographed after staining (a) and Sirtl etching (b). Figure 19a shows one white curved line and two white straight segments, which are due to enhanced diffusion. Figure 19b shows the same area after Sirtl etching, indicating that the enhanced diffusion occurred at a high-angle grain boundary (curved) and two straight segments of boundaries with heavy etched marks. In addition, there is a group of coherent twins and/or microtwins, appearing as lightly etched straight lines that cause no enhanced diffusion and appear to have an angular relationship to the two segments of boundaries having enhanced diffusion. The details of the relationship are discussed below.

Figure 20a shows an EBIC picture of a 1100°C-diffused Wacker sample in which three dark curved lines and one thin dark straight line appear. The three curved lines correspond to three high-angle boundaries with strong recombination activities. The origin of the thin line is not known; it contributes only a light recombination activity. Figure 20b is the surface appearance of the same area after grooving and staining, showing that the diffusion enhancement occurs at three boundaries with strong recombination

(a)

(b)

Figure 18. Image of Diffused n-Type Region Shown as the Brighter Region by Staining (a) and Image of Negatively Charged Phosphorus-Silicon Ions From the Same Area by SIMS (b)

(a)

(b)

Figure 19. Image of Enhanced Diffusion at Grain Boundaries, Shown as White Lines by the Staining (a), and Surface of the Same Region After Sirtl Etching (b)

(a)

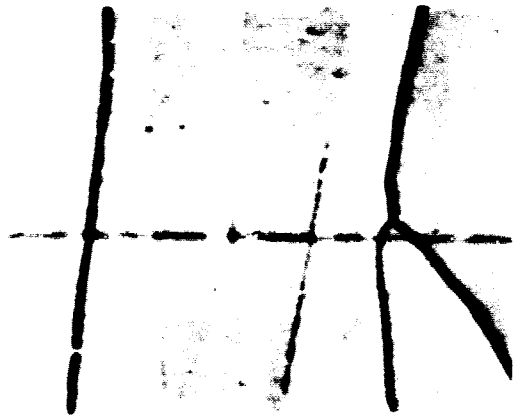

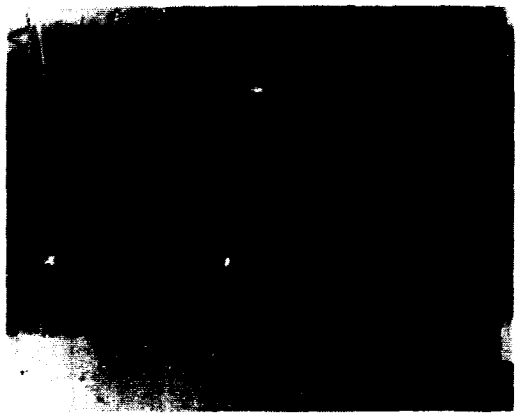

(b)

Figure 20. EBIC Image of a Wacker Sample (a); Image of Enhanced Diffusion at Grain Boundaries, Shown as White Lines by Staining (b)

activities, but not at one with weak recombination activity. These two pictures illustrate a generally observed fact from our study: grain boundaries capable of enhancing diffusion always show strong recombination activities, and the boundaries with weak recombination activities often contribute no observable enhanced diffusion. It should be mentioned that the sensitivity and resolution of the staining technique is poor in comparison with those of the EBIC experiments.

In those experiments, only samples of Wacker wafers diffused at 1100°C were used, because the enhanced diffusion was relatively deep (about 2 μm). The use of deep-diffused samples was necessary for the studies of the one-to-one correlations described above. Data concerning enhanced diffusion under normal solar-cell fabrication processes are presented below.

Samples of three cast polycrystalline photovoltaic materials (Wacker, HEM, and Semix) were diffused at 850°C for 30 min. More than 200 boundaries in each material were examined, using optical microscopy after staining and after Sirtl etching. Simple twins (including microtwins) and high-order grain boundaries were counted separately, because twins are easily distinguishable as straight lines, with no electrical or diffusion activities.

Only fractions of the total grain boundaries in the materials have observable enhanced diffusion after a typical solar-cell fabrication process. The detectability of the staining technique is about 0.05 μm. Figure 21 shows histograms of numbers of grain boundaries with observable enhanced diffusion as functions of measured enhanced diffusion depth beyond the bulk diffusion depth for the three materials. One general observation, common to all the materials, can be made: the distribution of the enhanced depth is reasonably broad, consistent with the fact that there are a large number of possible lattice mismatch configurations for grain boundary formation. All three distributions seem to be symmetrically centered about 0.3 μm, which is about the same as the bulk diffusion depth. The deepest penetrations at grain boundaries in the three materials beyond the bulk diffusion depth are the same, about twice the bulk diffusion depth. Table 2 presents numbers of twins, high-order grain boundaries, grain boundaries with observed enhanced diffusion, and average enhanced diffusion depth with standard deviation.

D. DISCUSSION

The groove-and-stain technique has been used for studying enhanced diffusion of phosphorus at silicon grain boundaries since the 1950s (Reference 17). Because it is a junction delineation technique, some ambiguity could exist in the identification of enhanced diffusion of phosphorus at the grain boundaries. In order to eliminate the ambiguity, a detailed correlation between the white lines observed in the stained and grooved surface and the image of phosphorus ions obtained by SIMS was performed. The result, as illustrated in Figure 18, indicates that the white lines appearing below the bulk diffusion region are in fact due to the enhanced phosphorus diffusion at grain boundaries.

Figure 19 illustrates the fact that high-angle boundaries are diffusion-active, whereas coherent twins are not. In addition, the figure also reveals a new observation, that $\{111\}/\{115\}$ second-order twins are diffusion-active. Since coherent twins and microtwins can be formed only in <111> lattice planes, the intersecting angle of two twins appearing on a surface can reveal the orientation of the crystals; e.g., the surface orientation is (110), when the intersecting angle is 70° 32'. That is the sample surface shown in Figure 19b. After the surface orientation is determined, the other orientation of the crystals consisting of twins and two segments of straight boundaries can be determined with the known twin properties. The result is presented in Figure 22, where a retracing of the boundary configuration of Figure 19b is shown. The material containing the twins are twinned crystals with two orientations, as marked by T1 and T2; both share a (110) surface plane. The straight lines marked B are coherent single twins or microtwins with an odd number of coherent twins. The upper segment of two straight boundaries with enhanced diffusion is an incoherent $\{111\}/\{115\}$ second-order

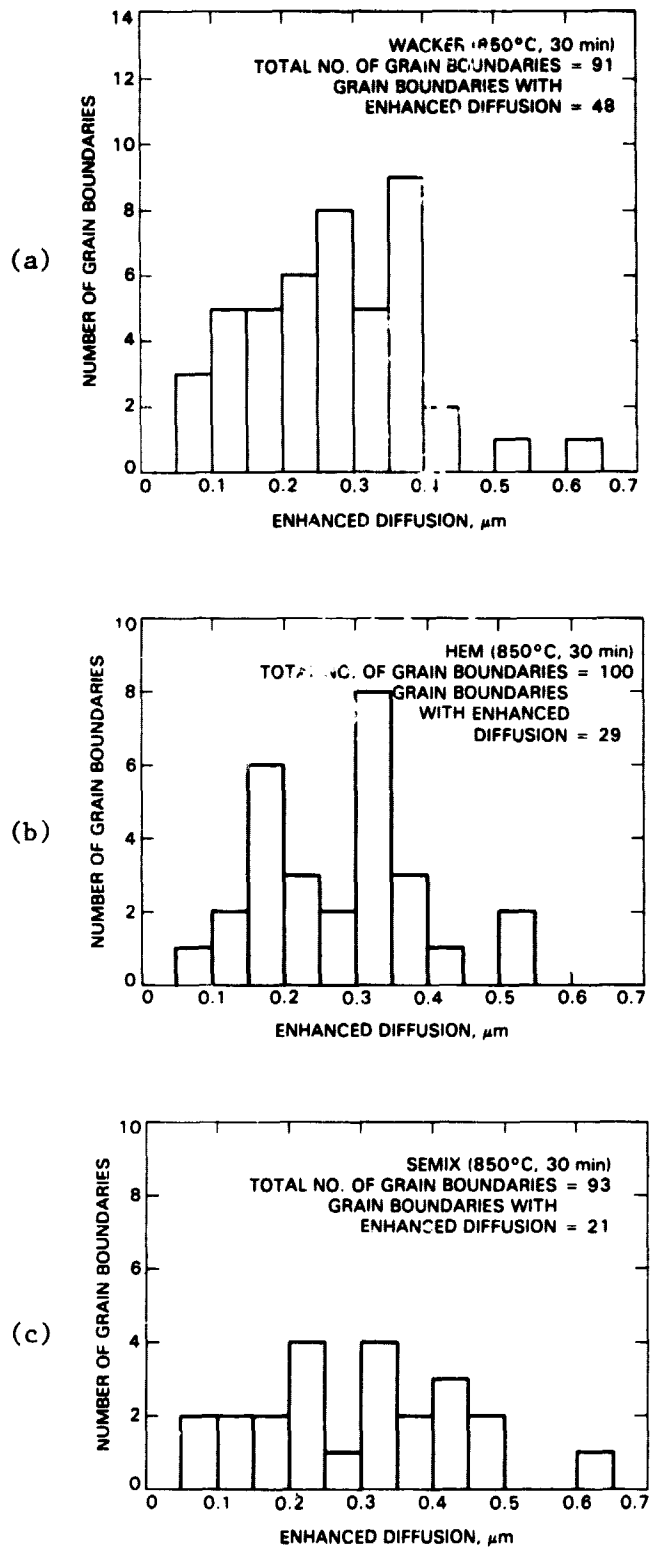

Figure 21. Histograms of Enhanced Diffusion in Wacker (a), HEM (b), and Semix (c) Samples

Table 2. Enhanced Diffusion of Phosphorus at Grain Boundaries in Wacker, HEM, and Semix Materials

	Wacker	HEM	Semix
No. of Twins	174	130	117
No. of Grain Boundaries	93	100	93
No. of Grain Boundaries with Enhanced Diffusion	45	29	21
Average Depth of Enhanced Diffusion (μm)	0.32	0.28	0.31
Standard Deviation (μm)	0.17	0.15	0.17

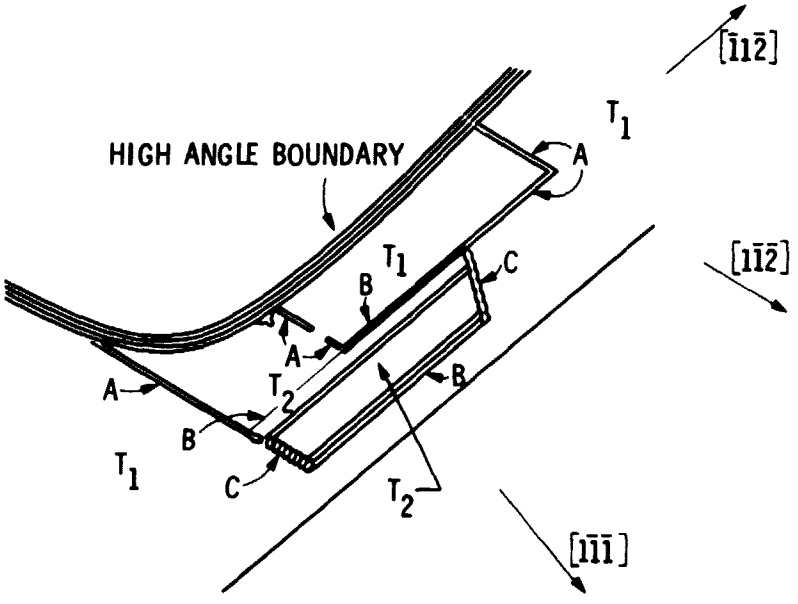

Figure 22. Schematic of Boundaries Shown in Figure 20b: A's Are First-Order Twins or Microtwins With Even Number of Coherent Twins; B's Are Single Coherent Twins or Microtwins With Odd Number of Coherent Twins; C's Are $\{111\}/\{115\}$ Second-Order Twins

twin, as determined from the intersecting angle with the nearby twins. The lower segment of the two straight boundaries could be a sequence of incoherent $\{111\}/\{115\}$ second order displaced gradually toward the T2 crystals, since the boundary is not aligned with the connecting microtwin, marked A. To conclude of the discussion of the features shown in Figure 19b: the present study has given the first experimental evidence that $\{111\}/\{115\}$ second-order twins are diffusion-active.

A recent transmission electron microscopy and EBIC study on EFG silicon ribbon material (Reference 19) has shown that incoherent second-order twins of $\{111\}/\{115\}$ type act as strong carrier recombination centers. The structural model of the $\{111\}/\{115\}$ interface set forth in Reference 20 reveals the existence of a large number of dangling bonds at the interface. Thus, there is a basis for speculation that the dangling bonds could be the source of the observed enhanced diffusion, similar to strong carrier recombination. The existence of unpaired dangling bonds can certainly help nearby silicon atoms make jumps at elevated temperatures. Consequently, the boundaries can act as vacancy sources that enhance diffusion in nearby material. This argument is consistent with the observed fact that the boundaries capable of enhancing the phosphorus diffusion always have strong recombination activities, as illustrated in Figure 20. The figure also indicates that the boundaries with weak recombination activities often contribute no observable diffusion.

Figure 22 shows three histograms as a function of the depth of the enhanced diffusion for Wacker, HEM, and Semix, respectively, after a typical solar-cell diffusion process (850°C for 30 minutes). The distribution of the enhanced diffusion depth for the three photovoltaic materials is reasonably broad, consistent with the fact that there are many possible lattice mismatch configurations for grain-boundary formation. However, it is interesting to observe from limited data that the average enhanced depth and the standard deviation are about the same for the three materials, as shown in Table 2. The average depths are around $0.3\,\mu m$ and the standard deviations are about $0.16\,\mu m$. The similarity reveals that the distribution of different types of grain boundaries capable of causing enhanced diffusion is the same for all the three materials. The similarity indicates that properties of grain boundaries are similar in all three materials, even though they are grown by three different methods. Table 2 shows that the ratio of the number of boundaries with enhanced diffusion to the total number of boundaries observed in Wacker samples (excluding twins) is higher than those of the other two materials. This could be because the grains in Wacker material generally are smaller.

The averaged depths of the enhanced diffusion for the three materials are about $0.3\,\mu m$, indicating that the effect of the enhanced diffusion on the solar cell performance is not a major one as far as increase of collection area is concerned. The data on the 1100°C diffusion shows that the average depth of the enhanced diffusion is about $2\,\mu m$, which is still not deep enough for a substantial increase of collection area. Some work to use diffusion of longer duration and at lower temperature has been mentioned (Reference 19). At present it is not clear how far the phosphorus can penetrate into the material under these conditions and how high the donor density can be. Those problems must be addressed in future work.

The recombination current at the junction is expected to be increased as a result of enhanced diffusion (References 21 and 22). This is a degrading effect of enhanced diffusion on solar-cell performance. It is not clear what its magnitude will be. Some encouraging approaches to correct the negative effects, such as grain boundary passivation by annealing in hydrogen atmosphere (References 23 and 24), have been attempted.

E. CONCLUSIONS

Enhanced diffusion of phosphorus at grain boundaries in three cast polycrystalline silicon photovoltaic materials were studied. It was found that enhancements in the three materials under typical diffusion conditions for solar-cell fabrication are the same with regard to the average enhanced depth and its statistical distribution.

The similarity indicates that properties of grain boundaries are similar in all three materials, even though they are grown by three different methods. In addition, it was found that the grain boundaries capable of enhancing diffusion always have strong recombination activities. Both phenomena could be related to the existence of dangling bonds at the boundaries. The present study gives the first evidence that incoherent second-order twins of $\{111\}/\{115\}$ type are diffusion-active.

REFERENCES

1. Seager, C.H., and Castner, T.G., J. Appl. Phys. 49, 3879, 1978.

2. Pike, G.E., and Seager, C.H., J. Appl. Phys. 50, 3414, 1979.

3. Seager, C.H., and Pike, G.E., J. Appl. Phys. Letters 35, 709, 1979.

4. Seager, C.H., Pike, G.E., and Ginley, D.S., Phys. Rev. Letters 43, 532, 1979.

5. Taylor, W.E., Odell, N.H., and Fan, H.Y., Phys. Rev. 88 , 867, 1952.

6. L. J. Cheng and C. M. Shyu, "Semiconductor Silicon/1981," ed. by H. R. Huff, R. J. Kriegler and Y. Takeishi, the Electrochemical Society, Pennington, New Jersey, 1981.

7. Card, H.C. and E.S. Yang, IEEE Trans. ED-24, 397 (1977).

8. Panayotatos, P., E.S. Yang, and Hwang, W., Solid-State Electronics, 25, 417 (1982).

9. Cheng, L.J., and Shyu, C.M., "Light Effects on Grain Boundary Properties in Silicon," Grain Boundaries in Semiconductors, Materials Research Society Symposia Proceedings, Vol. 5, Elsevier Science Publishing Co. Inc., New York, 1982.

10. Lang, D.V., J. Appl. Phys. 45, 3014, 1974; 45, 3023, 1974.

11. Rava, P., Gatos, H.C., and Lagowski, J., "Semiconductor Silicon/1981," ed. by H. R. Huff, R. J. Kriegler and Y. Takeishi, the Electrochemical Society, Pennington, New Jersey, 1981.

12. P. Panayotatos and H. C. Card, IEEE Electron. Device Lett. 1, 263 (1980).

13. C. H. Seager, J. Appl. Phys. 52, 3960 (1981).

14. J. G. Fossum and F. A. Lindholm, IEEE Trans. Ed-27, 692 (1980).

15. Shyu, C.M., and Cheng, L.J., "Electronic States Associated With Grain Boundaries in Silicon," Grain Boundaries in Semiconductors, Materials Research Society Symposia Proceedings, Vol. 5, Elsevier Science Publishing Co., New York, 1982.

16. Lindmayer, J., Proceedings of the 13th IEEE Photovoltaic Specialists Conference, p. 1092, 1978.

17. Quisser, H.J., Hubner, K., and Schockley, W., Phys, Rev. 123, 1245, and the references cited, 1961.

18. McDonald, B., and Goetzberger, A., J. Electrochem, Soc. 109, 141, 1962.

19. DiStefano, T.H., and Cuomo, J.J., Proc. NSF-ERD Workshop on Low-Cost Polycrystalline Silicon Solar Cells, p. 230, Southern Methodist University, Dallas, Texas, 1976.

20. Cunningham, B., Strunk, H., and Ast, D., Appl. Phys. Lett. 40, 237, 1982.

21. Storti, G.M., Johnson, S.M., Lin, H.C., and Wang, C. D., Proceedings of the 14th IEEE Photovoltaic Specialists Conference, p. 191, 1980.

22. Armstrong, R.W., Taylor, M.E., Stroti, G.M., and Johnson, S.M., Proceedings of the 14th IEEE Photovoltaic Specialists Conference, p. 196, 1980.

23. del Valle, J.L., Flores, C., and Suenas, F., Proceedings of the 14th IEEE Photovoltaic Specialists Conference, p. 202, 1980.

24. Seager, C.H., Ginley, D.G., and Zook, J.D., Appl. Phys. Lett. 36, 831, 1980.